Contents lists available at ScienceDirect

EBioMedicine

Research paper

A SNP of bacterial *blc* disturbs gut lysophospholipid homeostasis and induces inflammation through epithelial barrier disruption

Dayuan Zou[a], Jingwen Pei[a], Jianfeng Lan[a], Hong Sang[b], Hongjuan Chen[a], Haoliang Yuan[c], Di Wu[a], Yuanyuan Zhang[a], Yufang Wang[a], Dingyu Wang[a], Yujie Zou[a], Di Chen[a], Jianan Ren[d,*], Xiang Gao[a,*], Zhaoyu Lin[a,*]

[a] *State Key Laboratory of Pharmaceutical Biotechnology, Nanjing Drum Tower Hospital, MOE Key Laboratory of Model Animal for Disease Study, Model Animal Research Center, Nanjing University, Nanjing 210061, China*
[b] *Department of Dermatology, Jinling Hospital, Medical School of Nanjing University, Nanjing 210002, China*
[c] *State Key Laboratory of Natural Medicines and Jiangsu Key Laboratory of Drug Discovery for Metabolic Diseases, Center of Drug Discovery, China Pharmaceutical University, Nanjing 210009, China*
[d] *Department of General Surgery, Jinling Hospital, Medical School of Nanjing University, Nanjing 210002, China*

ARTICLE INFO

ABSTRACT

Background: Alteration of commensal bacterial composition is associated with many inflammatory diseases. However, few studies have pinpointed the specific bacterial genes that may suppress host immune responses against microbes and maintain homeostasis in the host intestine.
Methods: High-throughput screening was performed in *Caenorhabditis elegans* with a single gene knockout ut screening was performed in *Caenorhabditis elegans* with a single gene knockout *Escherichia coli* (*E. coli*) library and identified the immune suppression gene *blc*. The coding sequences of *blc* among different kinds of *E. coli* strains were aligned to identify the single nucleotide polymorphisms (SNPs). Physiological and biochemical experiments were performed in *C. elegans* and mice to explore the function of the *blc* variant.
Findings: By screening 3983 *E. coli* mutants, we discovered that 9 bacterial genes, when deleted, activate innate immunity in the host *C. elegans*. Among these 9 genes, the gene encoding *blc* showed a distinctive SNP in many clinically pathogenic bacteria. We found that bacteria with this SNP, which converts Blc ^{G84} to Blc ^{E84}, are highly enriched in the faeces of patients with inflammatory bowel disease (IBD). Exposure to Blc^{E84}-encoding bacteria resulted in epithelial barrier disruption and immune activation in both worms and mice. Detailed analysis indicated that infection with Blc^{E84}-encoding bacteria causes a significant decrease in LPE levels in the intestine and subsequently disrupts gut epithelial integrity in mice. Consistently, the levels of LPE in patients with IBD are significantly lower than those in healthy people. Finally, supplementation with LPE, which activates LPA$_1$/PLCβ/PKC signaling, reversed the defects induced by Blc^{E84}-encoding bacteria.
Interpretation: Our results identified a novel bacterial gene, *blc,* in *E. coli* that regulates host gut integrity and immunity.
Fund: The Ministry of Science and Technology of China; the National Natural Science Foundation of China; and the Natural Science Foundation of Jiangsu Province.

1. Introduction

The intestine serves as a major gateway for diverse microorganisms and dietary antigens. To meet the challenges of exposure to these potential pathogens, the gastrointestinal tract ensembles complicated mechanisms to keep the immune responses in check [1].

Intestinal inflammation is the most common response to pathogenic infection originating from the outside environment. Dysregulated immunity, such as in inflammatory bowel diseases (IBDs), is tightly associated with tumorigenesis, including colitis-associated colorectal cancer (CRC) [2]. The intestinal microbiota is crucial for regulating susceptibility to pathogens [3], maintaining alkalinity/acidity and oxygen concentration [4,5], and modulating the host immune system [6,7]. Pathogenic bacteria such as *Citrobacter rodentium* [5], *Helicobacter hepaticus* [8] and adherent-invasive *Escherichia coli* (AIEC)

* Corresponding authors.
E-mail addresses: jiananr@nju.edu.cn (J. Ren), gaoxiang@nju.edu.cn (X. Gao), Linzy@nju.edu.cn (Z. Lin).

Research in context

Evidence before this study

In the study of intestinal inflammation-related diseases represented by inflammatory bowel disease, dysbiosis of the gut microbiota, especially Enterobacteriaceae (including *Escherichia coli*), has been found. Furthermore, administration of tungstate to specifically downregulate the abundance of *Escherichia coli*, helps to alleviate the phenotype of intestinal inflammation, which suggests an important relationship between *Escherichia coli* and intestinal inflammation. Despite the numerous strains of *Escherichia coli*, few studies have reported whether there are specific bacterial genes that function in maintaining the homeostasis of the host intestine. Recently, via multiomics analysis, Jason lloyd-Price et al. found that lysophosphatidylethanolamine was significantly decreased in the faecal samples from patients who suffered from inflammatory bowel disease. However, the relationship between the downregulation of lysophosphatidylethanolamine and specific *Escherichia coli* genes in inflammatory bowel disease and the physiological function of lysophosphatidylethanolamine in intestinal homeostasis remains unknown.

Added value of this study

(1) We identified a conserved *blc* g251a variant that was enriched with different kinds of pathogenic *Escherichia coli* strains but was rarely found in non-pathogenic *Escherichia coli* strains.
(2) We found that, during inflammatory bowel disease, the expansion of *Escherichia coli* is mainly *blc*[a251] bacteria, while the relative abundance of *blc*[g251] bacteria showed a significant decrease.
(3) The *blc*[a251] gene increases bacterial pathogenicity and promotes the occurrence and development of intestinal inflammation.
(4) Our results suggest that the downregulation of lysophosphatidylethanolamine is associated with an increase in *blc*[a251] bacteria in patients suffering from inflammatory bowel disease.
(5) We demonstrate a protective function of lysophosphatidylethanolamine in sustaining the integrity of the intestinal epithelial barrier.

Implications of all the available evidence

Our study indicates that the *blc*[a251] variant could be used as an indicator for the diagnosis of inflammatory bowel disease, and could be helpful for the classification of inflammatory bowel disease subtypes to facilitate targeted treatment. Moreover, lysophosphatidylethanolamine is widely found in foods including rice and wheat, so supplementation with of lysophosphatidylethanolamine is safe and may also be helpful for remission of inflammatory bowel disease.

NC101 [9], promote intestinal inflammation and induce tumorigenesis. The host, conversely, imposes selective forces on bacterial growth throughout the inflammatory microenvironment. These forces, including iron limitation and the generation of reactive oxygen species and nitrogen species, influence the composition of gut-associated microbial communities [10].

E. coli is a dominant group of mammalian microbiota. There are more than 190 serotypes according to bacterial antigens, including flagellar antigens, somatic antigens and capsular polysaccharide antigens. At least four clinical syndromes are caused by *E. coli* serotypes, including diarrhea [11], septicaemia [12], urinary tract infection (UTI) [13] and some types of meningitis [14]. Among these diseases, diarrhea is a common symptom that affects the quality of life of billions of patients and causes millions of deaths every year [15]. Commonly, diarrhea is often caused by infection with microorganisms such as diarrheagenic *E. coli* [11].

Under healthy circumstances, there are approximately 10^{10}–10^{11} *E. coli* cells per gram in the human colonic content, with more than 500 serotypes in the uninflamed human intestine [16]. Interestingly, the host gut exhibits strong immune tolerance, showing minimal induction of inflammatory responses to common orally ingested antigens and a high density of commensal bacteria [17]. Some important observations have been made to explain why a high density of *E. coli* does not trigger a severe immune response. First, non-pathogenic *E. coli* lack pathogenicity islands (PAIs), which are horizontally transferred DNA sequences inserted into the core genome of the pathogen [18]. Second, the host intestinal epithelium shows polarized expression of many pattern recognition receptors (PRRs), such as Toll-like receptor 4 (TLR4) and nucleotide-binding oligomerization domain-containing protein 2 (NOD2), in only the basal layer and not in the epic layer [19]. Moreover, non-pathogenic *E. coli* may have the ability to protect the host intestine from inflammation [20,21].

We tried to screen the specific genes encoded by non-pathogenic *E. coli* that promote gut homeostasis and suppress inflammation by *C. elegans*. We hypothesized that specific bacterial genes may share a conservative function in regulating host-bacterial interactions. While we performed our studies, three independent groups reported genetic screens using the same strategy as the *E. coli* knockout library on *C. elegans* to explore the influences of bacterial composition on host longevity or responsibility to cancer chemotherapeutics [22–24].

With this screening protocol, we identified 9 candidate genes, including the bacterial lipocalin gene *blc*, that are required to suppress the immune response of non-pathogenic *E. coli* in worms. Furthermore, we found that the *blc* g251a (G84E) variant was highly enriched in faecal samples from patients with inflammatory bowel diseases (IBDs). Mice fed *blc*[g251a] *E. coli* displayed disrupted gut integrity and active inflammation. A detailed study indicated that the *blc* gene regulates host gut homeostasis through the LPE/ LPA$_1$/PLCβ/PKC axis.

2. Materials and methods

2.1. Screening strategy

Mutant strain ZD39 [agIs219 (T24B8.5p::GFP::unc-54-3' UTR + ttx-3p::unc-54-3' UTR) III; pmk-1 (km25) IV.] was obtained from the Caenorhabditis Genetics Center (CGC), and the reporter worm strain DCL15 [agIs219 III.] was generated in the laboratory. The agIs219 transgenic cassette contains a T24B8.5 promoter, which is an antimicrobial peptide (AMP) that is directly regulated by the PMK-1/ p38 mitogen-activated protein kinase (MAPK)-driven GFP expression reporter system. This transgenic *C. elegans* could be used to reflect the host immune activation state. Unless otherwise noted, the worms were maintained and experimentally tested at 20 °C on standard nematode growth medium (NGM) agar plates seeded with *E. coli*. Bacteria strains in the Keio library, which were inoculated into a 96-well plate that contained LB broth with kanamycin (59 ng/ml, Sangon Biotech Cat# A506636) by a 96-pin replicator and cultured for 22 h at room temperature. The *E. coli* medium was concentrated to approximately fifty microliters by Eppendorf centrifugation (5810R) at 4000 rpm for 5 min. The bacterial cells were then resuspended and seeded into PNGM (peptone-absent NGM) and stored at 4 °C in 24-well plates. The seeded 24-well plates were air dried in a hood before adding synchronized L1 stage reporter worms. Abnormal

fluorescence was scored at approximately 60 h (Nikon, Eclipse Ni-U upright microscope). Positive hits with observable upregulated intestinal GFP expression were picked up and then confirmed with three random experiments. The flowchart of the primary screening is illustrated in Fig. S1.

2.2. blc re-expression assay

Based on the prokaryotic plasmid pGEX-4T-3, we constructed a *blc* expression plasmid (pGEX-4T-3-*blc*). Both pGEX-4T-3-*blc* and pGEX-4T-3 were generated and amplified by *E. coli* DH5α before being electroplated into *E. coli* BW25113 and $\triangle blc$ by an electroporator (BIO-RAD, Gene Pulser Xcell^{TM}). Blc expression in reconstructed *E. coli* BW25113;*blc* and $\triangle blc$;*blc* were identified by the tailor-made antibody (Genscript, China).

2.3. Bacterial strains, culture conditions and E. coli growth curve

The *E. coli* Keio collection (Thermo Fisher Scientific, Cat# OEC4988) [25], the Keio knockout parental strain K-12 BW25113 (Thermo Fisher Scientific, Cat# OEC5042), OP50, DH5α and *P. aeruginosa* strain PA14 (a kind gift of Professor M.Q. Dong, NIBS, Beijing, China) have been described. Different kinds of *E. coli* strains were cultured overnight at 37°C in Luria broth (LB) medium and the *P. aeruginosa* strain was grown at 37 °C in King's broth medium [26].

The bacterial colonies were plated from glycerol stocks by plate streak, cultured on LB agar and incubated overnight at 37 °C. Single colonies were grown in 5 ml of LB broth overnight at 37 °C with shaking at 220 rpm. The inocula were diluted in fresh LB broth (1:500), and grown until the absorbance (OD600) reached 0.2. Then, the inocula were diluted 1:10,000 in 5 ml of fresh LB broth at 37 °C with shaking at 220 rpm (aerobic). Inocula were also diluted 1:10,000 in 15 ml of fresh LB broth in sterile 15 ml centrifuge tubes with Parafilm at 37 °C with shaking at 220 rpm (anaerobic). Bacteria were collected to measure the OD600 every half hour.

2.4. blc g251a point mutation

The coding sequences of *blc* in different *E. coli* strains were downloaded from EcoCyc *E. coli* database, and alignment analysis was performed by DNASTAR Lasergene. A SNP site at the 251st site that resulted in the G84E replacement was identified.

2.5. E. coli blc^{E84} construction

A reconstructed pSC101-λ RED plasmid that can induce RED recombinase expression by L-arabinose after precise incubation at 30 °C was a kind gift from Nanjing Biomedical Research Institute of Nanjing University. For *blc* gene g251a mutagenesis, the pSC101-λ RED plasmid was electroplated into *E. coli* BW25113 (BW25113;pSC) which was cultured at 37 °C to maintain plasmid expression. Linear kanamycin resistance cassette flanked with 50 bp homologous arms in which the 5' homology arm contains the *blc* g251a point mutation was transformed. The K$^+$ gene is used to select the positive *E. coli* strain that shows homologous recombination.

2.6. Mice and diets

Male C57BL/6N mice (D000274) from the Model Animal Research Center (MARC) of Nanjing University (Nanjing 210061, China) were chow-fed under specific pathogen-free (SPF) conditions in routine animal rooms or cofferdam tanks. Male ICR Germfree mice (N000293) from the Model Animal Research Center (MARC) of Nanjing University were fed under germfree conditions in cofferdam tanks. All animal experiments were performed with the approval of the Animal Research Committee of MARC (#MARC-GX84).

2.7. AVNM mouse construction and E. coli infection study

Five-week-old mice were transferred from the routine conditions to the cofferdam tank for one week before experiments to adapt to the housing conditions. After a 1-week adaptation to housing conditions, 6-week-old mice were gavaged daily with an aqueous antibiotic cocktail solution containing ampicillin (5 mg per mouse, Sangon Biotech Cat# A100339), vancomycin (5 mg per mouse, Sigma-Aldrich Cat# V2002), neomycin (5 mg per mouse Sangon Biotech Cat# A610366) and metronidazole (4 mg per mouse Sangon Biotech Cat# A600633) for 7 days. Then, the antibiotic cocktails were continuously administered for 7 days by dissolving them in drinking water (ampicillin 1 g/L, vancomycin 0.5 g/L, neomycin 1 g/L and metronidazole 1 g/L) [27].

AVNM mice aged 8 weeks were divided into 2 groups. Twenty-four hours after AVNM treatment, the *E. coli* BW25113 or *blc*^{E84} *E. coli* strain was intragastrically inoculated at a concentration of 1×10^8 colony forming units (CFU) per mouse in 200 µl of LB broth. On a specific day post-infection, mice were anaesthetized (with xylazine and ketamine) before blood collection and tissue dissection.

2.8. LPE/LPA supplement assay

AVNM mice infected with *E. coli* BW25113 or *blc*^{E84} were orally administered LPE (20 µM, 200 µL, dissolved in peanut oil, Avanti Polar Lipids Cat# 846725P) or Oleoyl-L-α-lysophosphatidic acid (LPA) (20 µM, 200 µL, dissolved in buffer solution: 118.4 mM NaCl, 4.7 mM KCl, 2.52 mM CaCl$_2$, 1.18 mM MgSO$_4$ and 25 mM Na gluconate, 1.18 mM KH2PO, 4, 25 mM Nagluconate pH 7.4, Sigma-Aldrich Cat# L7260) on day 0 post-infection. Control groups received the same volume of peanut oil or buffer solution [28].

2.9. Ki16425 treatment assay

AVNM mice infected with *E. coli* BW25113 or *blc*^{E84} were intraperitoneally injected with 20 mg/kg Ki16425 (MCE Cat# HY-13285) on day 0 post-infection. Control groups received the same volume of DMSO [29].

2.10. FITC-dextran assay

The FITC-dextran assay was performed as described [30]. For examination of colonic barrier function following *E. coli* infection, 0.1 ml of 80 mg/ml FITC-dextran (Sigma-Aldrich Cat# 46944-500MG-F) in PBS was introduced to mice by enema. Two hours after administration, serum was collected from the mouse orbital venous plexus and measured with a fluorescence microplate reader (MD, Flexstation 3).

2.11. Polychromatic FACS analysis

The distal colon tissue and spleen were isolated and digested with collagenase II (2 mg/ml, Worthington Biochemical Corp.) for 30 min in a 37 °C water bath. Resuspended cells were incubated with antibodies (0.2mg/ml each) at 4 °C for 1 h, after the removal of tissue residue and erythrocytes by a 70 µm sterile cell strainer (Fisher Scientific Cat# 22363548). The following Biolegend antibodies were used: CD11b-PE-CF594 (Cat# 301340), CD11c-PE-Cy7 (Cat# 301608), F4/80-BV605 (Cat# 123133), Ly6C-FITC (Cat# 128006), Ly6G-BV421 (Cat# 127628) and MHCII-APC-Cy7 (Cat# 107628) for panel 1; and antibodies were used CD3-PE (Biolegend Cat# 100206), CD4-APC (Biolegend Cat# 100412), CD8a-PE-CF594 (Biosciences Cat# 562283), CD19-BV510 (Biolegend Cat# 115546) and CD335-AF-647 (Biolegend Cat# 137628) for panel 2. Stained cells were analyzed by flow cytometry (BD, LSRFortessa^{TM}) and the data were analyzed using FlowJo software.

2.12. Blood biochemical analysis

Blood samples from mice were collected from the orbital venous plexus and clotted by standing on ice for 1.5 h. Serum was isolated by Eppendorf centrifugation (5810R) at 3000 rpm at 4 °C for 20 min and stored at -80 °C for long-term storage. Total protein (TP) and albumin (ALB) in serum were detected with a 7600 Clinical Analyzer (Hitachi High-Technologies, Japan).

2.13. Histopathology

Formalin-fixed tissue was embedded in paraffin and stained with F4/80 rat monoclonal antibody (Novus, NB600-404), CD11b rabbit polyclonal antibody (Novus Cat# NB110-89474), Ly-6G/Ly-6C rat monoclonal antibody (Novus Cat# NBP2-00441), E-cadherin rabbit monoclonal antibody (Cell Signaling Technology Cat# 3195), ZO-1 rabbit polyclonal antibody (Abcam Cat# ab59720), Occludin rabbit polyclonal antibody (Novus Cat# NBP1-87402) and Claudin-1 rabbit polyclonal antibody (Abcam Cat# ab15098).

2.14. blc^{E84}/blc^{G84} ratio assay

Fresh faecal samples from IBD and ophthalmology patients without oral antibiotic treatment were obtained with informed consent from patients according to the Declaration of Helsinki. In addition, the acquisition of faecal samples was approved by the Institutional Review Board of Jinling Hospital. The present study was approved by the Ethics Committee of the Medical School of Nanjing University. Written informed consent was obtained from all the patients enrolled in this study. Human faecal samples were collected from 12 ulcerative colitis (UC) patients (mean age ±SD: 35.67 ± 12.74 years; 3 females, 9 males; course of disease: from 1 month to 10 years; family history: 0; mildly active: 4, moderately active: 3, severely active: 2, clinical remission: 3; tobacco use history: 2; alcohol use history: 3) and 17 Crohn's disease (CD) patients (mean age ±SD: 23.59 ± 11.09 years; 2 females, 15 males; course of disease: from 1 month to 9 years; family history: 1; mildly active:2, moderately active: 2, severely active: 1, clinical remission: 12; tobacco use history: 1; alcohol use history: 0) were from the Department of General Surgery of Jinling Hospital, and samples from healthy subjects (mean age ±SD: 38.24 ± 10.08 years; 15 female, 10 males) were from the Department of Dermatology of Jinling Hospital. The faecal samples were collected with stool tubes and stored at -80°C immediately after labelling and flash freezing. The total bacterial DNA in the stool samples was isolated with a QIAamp DNA Stool Mini Kit (Qiagen Cat# 51504). Then, the blc^{E84}/blc^{G84} ratio was examined by a pair of primers (forward: CGCCGGTAAAGTACGCTTTC, reverse: CGGCCTGAATGTCATTAA-TAAAGG) and two TaqMan MGB probes (blc^{G84} FAM-CTGCCA-CATTCCT; blc^{E84} VIC-TGCCACATTTCTCTGT) (Thermo Fisher Scientific, 431603401).

2.15. Cell line and culture conditions

The human epithelial cell line Caco-2, which was kindly provided by the Stem Cell Bank, Chinese Academy of Sciences, was plated in growth medium [minimum essential medium (MEM) (HyClone Cat# SH30265.01) supplemented with 20% FBS (v/v) (PAN-Seratech Cat# ST30-3302), 100 μg/mL streptomycin and 100 units/mL penicillin (ThermoFisher Cat# 15140)]. The cells were cultured in a humidified incubator at 37 °C with 5% CO$_2$. Caco-2 cells were pre-treated with H$_2$O$_2$ (50 μM) for 8 h to induce oxidative stress. LPA (1 μM) or LPE (20 μM) was in the presence or absence of protein inhibitors, including AM095 (MCE Cat# HY-16039), Ki16425 (MCE Cat# HY-13285), HA130 (MCE Cat# HY-19329), GLPG1690 (MCE Cat# HY-101772) and GF-109203X (Sigma-Aldrich Cat# G2911), at different concentrations for 24 h.

2.16. siRNA knockdown

Caco-2 cells at a concentration of 5×10^6 were transfected with siRNA specific for $Plc\beta 1$, $Plc\beta 2$, and a non-targeting siRNA (siCTRL) (purchased from GenePharma, China) with the Neon Transfection System (ThermoFisher) (1400 V, 20 ms, 1 pulse number).

2.17. C. elegans intestinal permeability assay

Worms were prepared as described for genomic screening. Synchronized germ-free worms were added to *E. coli* BW25113- or *E. coli* blc^{E84}-seeded NGM and cultured at 20°C for 57h. Then, ~10 synchronized animals were moved to an aqueous solution of Erioglaucine disodium salt (FD&C Blue #1, Sigma-Aldrich Cat# 861146) at 75 mg/ml and suspended for 2 h at room temperature. Worms were then placed onto blank NGM plates and examined for blue dye with a microscope (Nikon, Eclipse Ni-U Upright Microscope) under $40 \times$ magnification. Three independent experiments were carried out, each with 8−10 animals per strain. Data were analyzed using GraphPad Prism.

2.18. C. elegans total protein extraction

Total protein extraction from *C. elegans* followed the next protocol. Approximately 500 worms were collected (2000 worms for phosphorylated p38 examination) at 60 h, and the bacteria were cleaned with S buffer (NaCl 100 mM, K$_2$HPO$_4$ 5.7 mM, and KH$_2$PO$_4$ 44 mM). The worms were washed with PBS twice then with deionized water (Millipore Cat# QGARD00R1) twice. The worms were resuspended in cold homogenization buffer (15 mM HEPES, 10 mM KCl, 1.5 mM MgCl$_2$, 0.1 mM EDTA, 0.5 mM EGTA, 44 mM sucrose, and 1 mM DTT) containing proteinase inhibitor cocktail (Sigma-Aldrich Cat# P8340), PMSF (100 mM), NaF (100 mM), and NaVO$_4$ (100 mM). The mixture was vortexed at 4°C for 1 h after sonication (6 pulses total for 3s at 210 W each time with 45 s between each cycle, SONICS, VCX500/ VCX750).

2.19. Western blot and antibodies

Whole cell lysates were prepared on ice plates using RIPA lysis buffer with protease and phosphatase inhibitors (150 mmol/L NaCl, 50 mmol/L Tris-HCl (pH 7.4), 0.1 mmol/L EDTA, 1% Nonidet P-40, 0.4 mmol/L phenylmethylsulfonyl fluoride, 1 mmol/L dithiothreitol, 0.1 mmol/L Na3VO4, 0.1 mmol/L NaF and protein inhibitor cocktail). Cell debris was removed by centrifugation, and the supernatant was heated to 95 °C for 5 min in loading buffer containing 5% β-mercaptoethanol. Then, the protein samples were subjected to SDS−PAGE, and the fractionated proteins were transferred to PVDF membranes (Amersham Bioscience). Protein blots were blocked with 5% fat-free milk at R.T. for 1 h and then incubated with a specific primary antibody O/N at 4 °C. After being washed with TBST, the protein blots were incubated with a specific secondary antibody for 1 h at R.T. Proteins were visualized using a chemiluminescent substrate. ImageJ software (NIH) was used for greyscale analysis.

Activated p38 rabbit polyclonal antibody (Promega Cat# V1211) could detect the TGY phosphorylated sites and the β-actin polyclonal rabbit antibody (Cell Signaling Technology Cat# 4967), which was used as a loading control in the *C. elegans* protein sample. E-cadherin rabbit monoclonal antibody (Cell Signaling Technology Cat# 3195), Occludin rabbit polyclonal antibody (Novus Cat# NBP1-87402), Claudin-1 rabbit polyclonal antibody (Abcam Cat# ab15098), and GAPDH mouse monoclonal antibody (Sigma Cat# G8795) were used as loading controls in the mouse protein samples.

2.20. Quantitative PCR analysis

For gene transcription level analysis, RNA was extracted with TRIzol (Takara Cat# 9109), and the cDNA template was reverse transcribed using the PrimeScript™ RT reagent kit (Perfect Real Time) (Takara Cat# RR047A). Quantitative real-time PCR (qPCR) was performed with a SYBR® Premix Ex Taq™ kit (Takara Cat# RR420A) in an ABI PCR machine (ABI, StepOne Plus™ System). Beta-actin was used as the internal control to normalize the target gene expression level. All data shown represent three biologically independent samples. Data were analyzed using GraphPad Prism. Statistical analysis was performed using Student's *t* test.

2.21. Homology modeling and molecular dynamics simulations

Since there is no available crystal structure of the protein Blc (bacterial lipocalin), homology modeling was performed to predict the 3D (three-dimensional) structure. A crystal structure (PDB ID: 3MBT) with a sequence identity of 98.74% was selected as the template. SWISS-MODEL [31] was applied for homology modeling. Molecular dynamics simulations were further used to minimize this model with a duration of 20 ns. Based on the final model, Gly84 was mutated to Glu84 manually with the *protein edit* tool in Accelrys Discovery Studio 3.0. This mutated model was also minimized with a molecular dynamics simulation of 20 ns. All molecular dynamics simulations were performed using AMBER 10.0 software package with the ff99SB force field [32]. The RESP fitting technique in AMBER was used to determine the partial charges. The general the AMBER force field (GAFF) and the LEaP module were used to address the protein. Each protein was immersed in a cubic box with the TIP3P water model and a 10 Å minimum solute-wall distance [33]. Each system was neutralized with different numbers of Cl ions. Energy was minimized in the solvated system employing 2500 steps of the steepest descent algorithm and 2500 steps of the conjugate gradient algorithm with a nonbonded cutoff of 10 Å. The protocol consisted of gradual heating, density equilibration, equilibration and production procedures in an isothermal isobaric ensemble (*NPT, P* = 1 atm and T = 298 K) MD. The system was gradually heated from 0 to 298 K over 50 ps, followed by density equilibration at 298 K for 500 ps, and then constant equilibration at 298 K for 500 ps. Then each system underwent a process of equilibration until the system achieved a continuous stable status, i.e., the production stage. The time step was set to 2 fs while the snapshots were taken every 10 ps to record the conformational trajectory during production MD. The nonbonded interactions were treated with a 10 Å cutoff [34]. The SHAKE algorithm was applied to constrain all bonds involving hydrogen atoms to their equilibrium length. Snapshots of the equilibrium state were collected every 50 ps for analysis [35].

2.22. Protein expression and purification

The *blc*^g251 and *blc*^a251 genes were subcloned into the pCold cold-induced expression plasmid III. The expression strategies for this experiment have been described. The coding sequence of the *blc* gene started from the 19th residue (cysteine), which fused with a GST tag and thrombin linker on the N-terminus. The absence of the type-2 secretory signal peptide of *blc* led to a soluble protein. This reconstructed *blc* gene sequence was expressed in the BL21 (DE3) *E. coli* strain. The GST tag was removed from the purified Blc^G84 and Blc^E84 by thrombin (Sangon Biotech Cat# C600413), and the purified proteins were desalinated with a 3KD ultrafiltration device (Millipore Cat# UFC500308).

2.23. Lipid pull-down analysis

Extraction of the total lipids followed the method of Bligh and Dyer with Cl_2CH_2: MeOH (2:1). To avoid the bias of lipid classes and concentration caused by the Blc protein variant, total lipids of *E. coli* Δblc were extracted and incubated with purified Blc^G84 or isometrical Blc^E84 at 4 °C for 12 h as described [36]. Protein A agarose beads pre-treated with a specific tailor-made Blc antibody were used to pull down the Blc-lipid complex. The lipids were purified by removing the agarose beads-protein A-Blc antibody-Blc complex via centrifugation at 2000 rpm at 4 °C for 5 min after DTT and $ClCH_2$ treatment. The dissolved lipids were dried with nitrogen gas in Cl_2CH_2: MeOH (2:1). LC-MS/MS analysis was performed to detect the lipid classes.

2.24. Non-reducing gel analysis

The non-reducing gel assay was performed as described [37]. The purified protein was mixed with loading buffer without β-mercaptoethanol and separated by SDS-PAGE. Dithiobis (succinimidyl propionate) (DSP) functioned as the protein crosslinker.

2.25. Blc dimer liquid chromatography-mass spectrometry (LC-MS) analysis

High performance liquid chromatography analysis was carried out with an LC-30AD system (Shimadzu, Japan). The purified protein samples in PBS were held at room temperature, and the injection volume was 10 μl. The chromatography column was an Agilent Poroshell 300SB-C8 (1.0 × 75 mm, 5 μm). The flow rate was 0.3 ml/min in gradient mode with 0.1% formic acid (A) and acetonitrile (B). The equilibrium time after the run was 25 min. Gradient conditions were as follows: 0−5.0 min, 5% B; 5.0−20.0 min, 5%−80% B; 20.0−25.0, 80% B. The column temperature was maintained at 60 °C. Mass spectral analysis was performed on a Triple TOF 4600 mass spectrometer (Sciex, America) equipped with an electrospray ionization (ESI) source and operated in positive ion mode. A calibration solution was used to calibrate the instrument. The curtain gas (CUR), nebulizer gas (GS1) and turbo gas (GS2) were set at 35 psi, 55 psi and 55 psi, respectively. The electrospray voltage was 5.5 kV, and the turbo ion spray source temperature was 550 °C. Nitrogen was employed as the collision gas. The mass spectrometer operated in the TOF-MS full scan mode with a 500−4000 m/z range. Data acquisition was performed using Analyst 1.6.2 software (Applied Biosystems). The Bayesian protein reconstruction tool was used to calculate protein molecules.

2.26. Lipid LC-MS/MS analysis

Fresh faecal samples from IBD and ophthalmology patients without oral antibiotic treatment were obtained with informed consent from patients according to the Declaration of Helsinki. In addition, the acquisition of faecal samples was approved by the Institutional Review Board of Jinling Hospital. The present study was approved by the Ethics Committee of the Medical School of Nanjing University. Written informed consent was obtained from all the patients enrolled in this study. Human faecal samples were collected from 12 UC patients (mean age ±SD: 35.08 ± 13.69 years; 5 female, 7 males; course of disease: from 2 months to 6 years; family history: 0; mildly active: 4, moderately active: 3, severely active: 1, clinical remission: 4; tobacco use history: 0; alcohol use history: 0) and 12 CD patients (mean age ±SD: 29.58 ± 12.53 years; 3 females, 9 males; course of disease: from 1 month to 9 years; family history: 0; mildly active: 1, moderately active: 2, severely active: 1, clinical remission: 8; tobacco use history: 1; alcohol use history: 1) from the Department of General Surgery of Jinling Hospital and from healthy subjects (mean age ±SD: 35.46±11.04 years; 12 females, 12 males) from the Department of Dermatology of Jinling Hospital. The faecal samples were collected with stool tubes and stored at -80°C immediately after labeling and flash freezing. The total lipids were extracted from stool samples and then subjected to LC-MS/MS analysis.

A UPLC system (Shimadzu LC-30AD) was used. Reversed-phase separation was performed on an Accucore C18 column (2.1 × 150 mm 2.6 μm; Thermo). The mobile phase consisted of (A) ACN/MeOH/10 mM NH4FA (50/50/50, v/v/v) and (B) ACN/IPA (50/50, v/v). Gradient elution without splitting was carried out for 20 min at a flow rate of 0.4 ml/min. Gradient conditions were as follows: 0−5.0 min, 10%−30% B; 5.0−10.0 min, 30%−80% B; 10.0−15.0 min, 80%−98% B; 15.0−20.0, 98% B. A 5 μl aliquot of each sample was injected into the column. The column temperature was maintained at 55 °C. All samples were incubated at 4°C during analysis. Mass spectrometry was performed on a Sciex 4600 Triple TOF mass spectrometer equipped with an electrospray ionization (ESI) source. Lipids were detected in positive ion mode. The curtain gas (CUR), nebulizer gas (GS1) and turbo gas (GS2) were set at 35 psi, 55 psi and 55 psi, respectively. The electrospray voltage was 5.5 kV, and the turbo ion spray source temperature was 550 °C. Nitrogen was employed as the collision gas. (For negative ion mode: curtain gas (CUR), nebulizer gas (GS1) and turbo gas (GS2) were set to 35 psi, 55 psi and 55 psi, respectively, the electrospray voltage was -4.5 kV, and the turbo ion spray source temperature was 550°C.) The mass spectrometer was operated in information-dependent acquisition (IDA) scan mode. The TOF-MS and MS/MS ranges were set at 200−1300 m/z and 100−1300 m/z, respectively. Data acquisition was performed using Analyst 1.6.2 software (Applied Biosystems). Lipid-View software (Applied Biosystems) was used to identify all lipids.

2.27. Statistics

Data were statistically analysed using two-tailed Student's t test or Mann−Whitney U test. For multiple comparisons, the p-values were adjusted by the p.adjust method (Benjamini & Hochberg) in R to exclude false positives/negatives. FACS data and qRT-PCR data are expressed as the mean ± SEM, and all other data are presented as the mean ± SD. Values of $p < 0.05$ were considered statistically significant.

2.27.1. Role of the funding source

3. Results

3.1. E. coli blc suppresses the C. elegans immune response

To identify microbial factors that may influence host innate immunity, we conducted a genetic screen by feeding a *C. elegans* reporter strain, DCL15, with individual mutants of the *E. coli* single-gene knockout library (Fig. S1) [25]. This worm strain carries the agIs219 transgene driving green fluorescent protein (GFP) expression under the promoter of a PMK-1/p38 mitogen-activated protein kinase (MAPK)-regulated antimicrobial peptide gene, T24B8.5 [38]. The parental strain of this bacterial knockout library, *E. coli* K-12 BW25113, was used as the experimental control. Among 3983 bacterial knockout mutants, we found that null mutants of nine genes significantly induced an innate immune response in *C. elegans*.

We next focused on the bacterial lipocalin gene (*blc*), which encodes a membrane protein. The Δblc *E. coli* strain induced worm innate immune activation as indicated by GFP expression in the intestine (Fig. 1a), along with upregulated AMP mRNA (*T24B8.5, K04F1.9, F08G5.6, F01D5.5, Y54G2A.5* and *K08D8.5*) and increased PMK-1 phosphorylation (Figs. 1b−d and S2a−d) [38]. Consistently, these phenotypes were rescued by transfection of a plasmid carrying the *blc* expression cassette (Fig. 1a−d). As a control, the PMK-1/p38-null worm strain ZD39 showed no intestinal GFP expression after feeding

with *E. coli* Δblc (Fig. S2e). These results confirmed that the *blc* gene is crucial for the immune tolerance of K-12 *E. coli* BW25113 in worms.

3.2. The pathogenic E. coli variant blc g251a (Blc G84E) is highly enriched in the faeces from patients with IBD

By comparing the *blc* coding sequences between non-pathogenic and pathogenic *E. coli* strains in databases [39,40], we found a conserved *blc* g251a variant in 21 of 25 pathogenic *E. coli* strains but rarely in the non-pathogenic *E. coli* strains, including K-12 *E. coli* BW25113 (Fig. 1e and f). The *blc* g251a variant resulted in a glycine-to-glutamic acid change at the 84th site in the amino acid sequence, from Blc^G84 to Blc^E84. Among these 25 pathogenic *E. coli* strains, 17 could induce host intestinal inflammation, and the strains NRG 857C and LF82 have been reported as the Crohn's disease-associated AIEC [41,42]. We also provided the overall prevalence of Blc variant among sequenced *E. coli* strains (Table S1). Among 555 sequenced *E. coli* strains, 251 strains contain the protein Blc^E84, while 304 strains contain the protein Blc^G84. Moreover, intestinal inflammation in IBD is frequently associated with dysbiosis with Enterobacteriaceae, so we analyzed the relative abundance of Blc^E84-containing bacteria in the faecal samples from patients with IBD and healthy controls. All faecal samples were collected from the patients without oral antibiotic treatment from the Department of General Surgery (IBD group, including 4 mildly active, 3 moderately active, 2 severely active, 3 clinical remission ulcerative colitis (UC), and 2 mildly active, 2 moderately active, 1 severely active, 12 clinical remission Crohn's disease (CD)), and the Department of Ophthalmology (control group, 25 healthy subjects) of Jinling Hospital, Nanjing, China. We found that the blc^E84/blc^G84 ratio was significantly higher in faecal samples from patients with IBD than in those from the control group (Fig. 1g). In detail, the blc^E84/blc^G84 ratio both in CD and UC patients showed significant differences compared with that of the control group (Fig. S3a). There were no remarkable differences in gender or age between the IBD group and the control group. These results suggest that pathogenic *E. coli* with the g251a variant is enriched in inflamed host intestines.

3.3. Infection with E. coli blc^E84 activates the host immune response in worms and mice

To confirm the pathogenic effects of the *E. coli blc* g251a variant, we constructed a *blc* g251a knock-in *E. coli* strain blc^E84 on the paternal K-12 *E. coli* BW25113 background using a modified RED-ET system. Then, we examined the abilities of both *E. coli* BW25113 and *E. coli* blc^E84 to cause an immune response in worms. Indeed, the *C. elegans* fed with *E. coli* blc^E84 displayed upregulated intestinal GFP expression (Fig. 2a), indicating the activation of immunity. AMP transcription (Fig. 2b) and PMK-1 phosphorylation levels (Fig. 2c) also increased in worms fed *E. coli* blc^E84.

Next, we tested the pathogenic effects of *E. coli* blc^E84 in mice. To reduce the potential interference of the complexity of the gut microbiota, mice were pre-treated with antibiotic cocktails containing ampicillin, vancomycin, neomycin and metronidazole (AVNM) [27]. These mice were then infected with *E. coli* BW25113 or *E. coli* blc^E84 at 1×10^8 colony-forming units (cfu) by oral-intragastric inoculation. *E. coli* blc^E84 induced diarrhea in mice 7 days post-infection (Table S2). Transcription of inflammatory cytokines including *Tnfα, Il1β, Il4, Il8* and *Il17* (Fig. 2d), and the genes of antimicrobial defense proteins including Reg3 and Cryptdin (Fig. S4a and b), were upregulated in the colon tissues of *E. coli* blc^E84-infected mice compared to those in the *E. coli* BW25113-infected group. Consistently, immunostaining in the distal colon showed a significant increase in the infiltration of F4/80^+, CD11b^+ and Ly-6G/6C^+ cells in the *E. coli* blc^E84-infected group (Figs. 2e and S4c−e). The gating strategy is shown in Table S3. The number
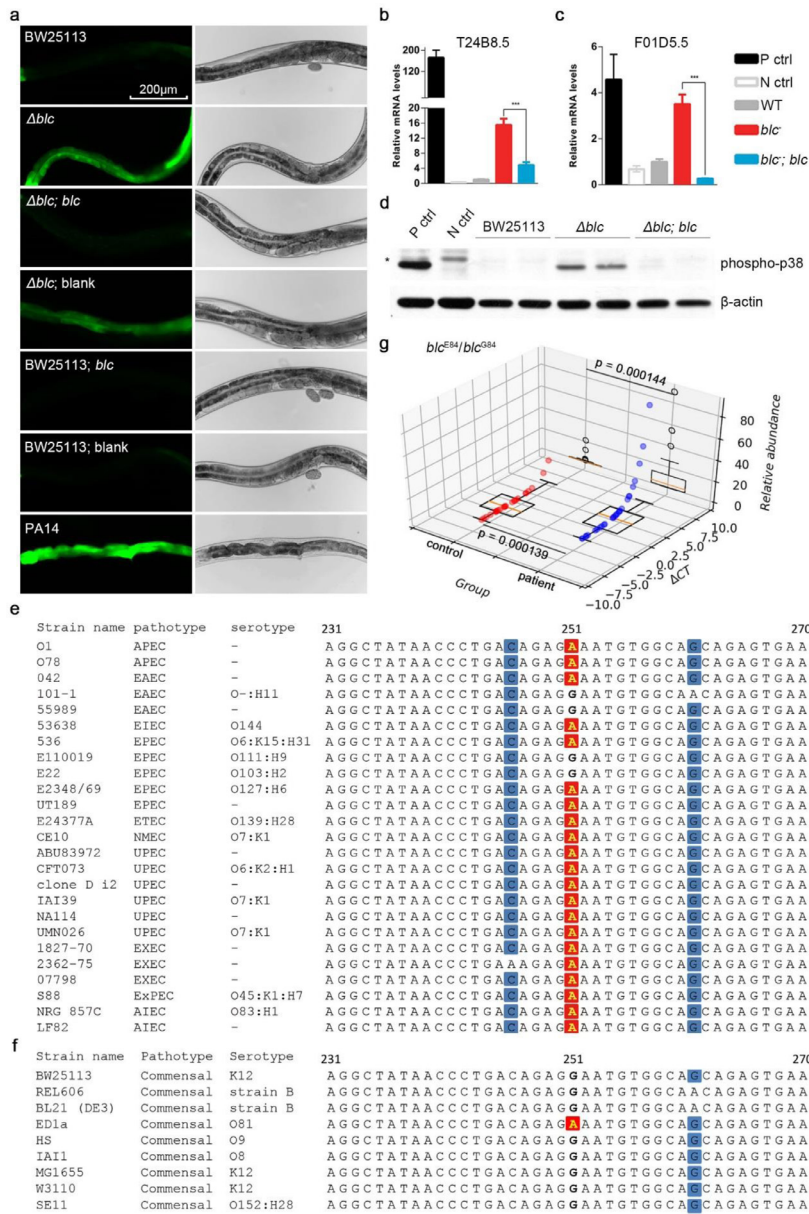
Fig. 1. The non-pathogenic *E. coli* variant *blc*[g251] (Blc[G84]) suppresses the *C. elegans* immune response, and variant *blc*[a251] (Blc[E84]) is enriched in pathogenic *E. coli* strains and faeces from patients with IBD. (a) Fluorescence and bright-field images of GFP expression driven by the promoter of AMP encoding the *T24B8.5* gene in young adult worms fed BW25113, Δ*blc*, Δ*blc;blc* (*blc*-re-expressing *E. coli* Δ*blc* strain), Δ*blc*;blank (blank vector-re-expressing *E. coli* Δ*blc* strain), BW25113;*blc* (*blc*-re-expressing *E. coli* BW25113 strain), BW25113; blank (blank vector-re-expressing *E. coli* BW25113 strain), or pathogenic PA14 bacteria. The scale bar represents 200 μm. (b and c) qRT-PCR analysis of AMP-encoding mRNAs of metridin-like ShK toxins T24B8.5 (b) and F01D5.5 (c) in worms treated with different bacterial strains. Error bars represent the mean ± SEM. (three biological replicates). *** $p < 0.001$ (two-tailed Student's *t* test and p.adjust with Benjamini & Hochberg). (d) Western blot analysis of phosphorylated PMK-1/p38 in worms treated with BW25113, Δ*blc* or Δ*blc;blc* bacterial strains. β-actin served as the internal control for equal loading. (e and f) Alignment of bacterial lipocalin genes from 25 pathogenic *E. coli* strains (e) and nine non-pathogenic commensal *E. coli* strains (f). The 251 adenine variants are highlighted in red, and synonymous mutations are highlighted in blue. (g) Human IBD patient faecal samples show significant enrichment of bacteria carrying the Blc[E84] variant over Blc[G84] (controls, n = 25; patients, n = 29). The difference in the CT between the two groups showed significant differences in the xy plane. The box plots in the xz plane display the CT value as an index of amplification efficiency for exponential operation. The calculation data of the CT value indicates the ratio of the relative abundance between *E. coli blc*[G84] and *E. coli blc*[E84] (Mann–Whitney U test). (For interpretation of the references to color in this figure legend, the reader is referred to the web version of this article.)

of CD4^{+} and CD8^{+} T cells was also significantly increased in the colonic tissue of the *E. coli blc*[E84]-infected mice by FACS analysis (Fig. 2f and g and Table S4). All of these observations indicated activated local inflammation in the gut after *E. coli blc*[E84] infection.

In addition to local inflammation, systemic inflammation was also activated by *E. coli blc*[E84] infection. Most types of immunocytes from spleen tissue and whole blood were increased (Figs. 2h−o and S5), including neutrophils (Figs. 2h and i and S5i and j), macrophages (Fig. 2j and k), monocytes (Fig. S5c, d, k and l), eosinophils (Fig. S5a, b, m, and n), CD4^{+} T cells (Figs. 2n and o and S5s and t), and NK cells

(Fig. S5v and w). However, CD8^{+} T cells (Fig. S5e, f, s and u) showed no significant differences. In summary, *E. coli blc*[E84] infection can induce an immune response in mice at the colonic and systemic levels 7 days post-infection.

3.4. Infection with E. coli blc[E84] disrupts the host intestinal epithelial barrier

IBDs are pathologically characterized by both chronic gastrointestinal inflammation and sustained epithelial injury [43]. Therefore, we
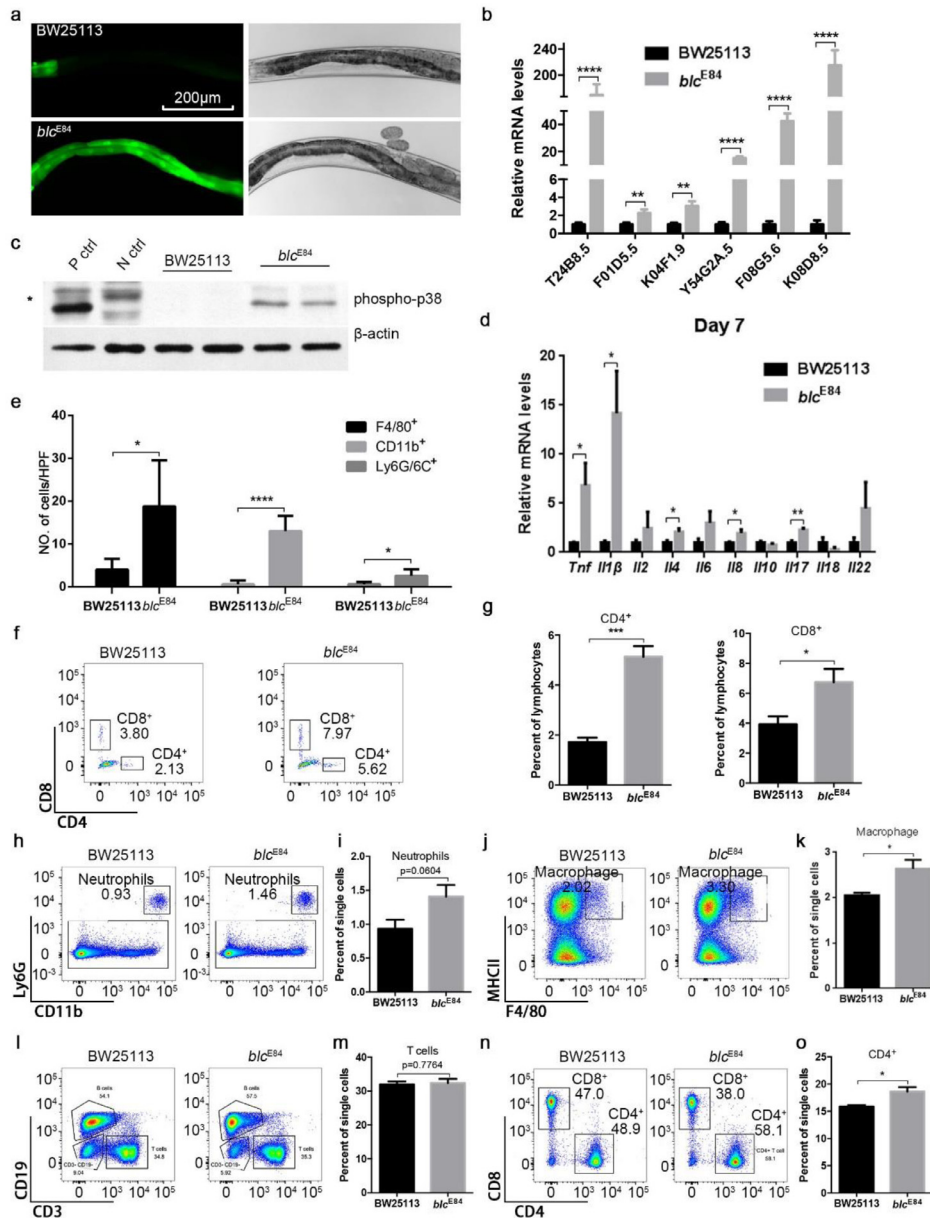
Fig. 2. *E. coli blc*[E84] activates the immune response in *C. elegans* and mice. (a) Fluorescent and bright-field images of the *T24B8.5* promoter driving GFP reporter expression in worms treated with *E. coli* BW25113 or *E. coli blc*[E84]. The scale bar represents 200 μm. (b) qRT-PCR analysis of AMP-encoding mRNAs in worms treated with *E. coli* BW25113 or *E. coli blc*[E84]. Error bars represent the mean ± SEM. **$p < 0.01$, ****$p < 0.0001$ (two-tailed Student's *t* test). (c) Western blot analysis of phosphorylated PMK-1/p38 levels in worms treated with *E. coli* BW25113 or *E. coli blc*[E84]. Animals treated with PA14 and the *pmk-1* null mutant treated with BW25113 served as the positive control (P ctrl) and negative control (N ctrl), respectively. *β*-actin served as the internal control. (d–o) Male C57BL6/N mice at 8 weeks old, which had been pre-treated with an antibiotic cocktail (AVNM mice), were gavaged with *E. coli* culture (10^8 cfu) once. Mice were sacrificed on day 7 post-infection (n = 5). (d) qRT-PCR analysis of *Tnf, Il1β, Il2, Il4, Il6, Il8, Il10, Il17, Il18* and *Il22* in the mouse distal colon (three biological replicates). Error bars represent the mean ± SEM. *$p < 0.05$, **$p < 0.01$ (two-tailed Student's *t* test). (e) Quantification of cell numbers (high power field) in Fig. S6. Error bars represent the mean ± SD. *$p < 0.05$, ****$p < 0.0001$ (two-tailed Student's *t* test). (f and g) Dot plots (f) and quantification (g) of CD4^{+} and CD8^{+} T cells in the whole distal colon from infected mice. Error bars represent the mean ± SEM. *$p < 0.05$, ***$p < 0.001$ (two-tailed Student's *t* test). (h–o) Dot plots and quantification of neutrophils (h and i), macrophages (j and k), T cells (l and m) and CD4^{+} T cells (n and o) in the spleens of infected mice. Error bars represent the mean ± SEM. *$p < 0.05$ (two-tailed Student's *t* test).

next examined the colon epithelial barrier integrity in animals exposed to *E. coli blc*[E84].

C. Elegans feeding on different *E. coli* strains were stained by FD&C Blue No. 1 dye, which can only penetrate the damaged gut epithelium [44]. The dye was restricted to the inside of the intestines of worms fed *E. coli* BW25113 (Fig. 3a, top). In contrast, the dye diffused throughout the whole body of worms fed *E. coli blc*[E84], indicating intestinal barrier disruption and leakage (Fig. 3a, bottom). In mice, we measured the integrity of the intestinal barrier indirectly by examining the serum levels of total protein (TP) and albumin (ALB) [45]. Mice infected with *E. coli blc*[E84] displayed much lower levels of

TP and ALB than mice infected with BW25113, indicating disruption of the intestinal barrier (Fig. 3b and c).

Adherens junction (AJ) proteins and tight junction (TJ) proteins are crucial to maintaining normal intestinal barrier function. Abnormal expression and localization of these proteins can result in altered intestinal permeability [46]. Western blots showed that the AJ protein E-cadherin and the TJ proteins Occludin and Claudin-1 were significantly downregulated in the colon tissues of *E. coli blc*[E84]-infected mice at day 7 post-infection (Fig. 3d and e). This result was confirmed by immunostaining that *E. coli blc*[E84] infection induced lower expression of enterocyte junction proteins (Figs. 3f and g and S6). These
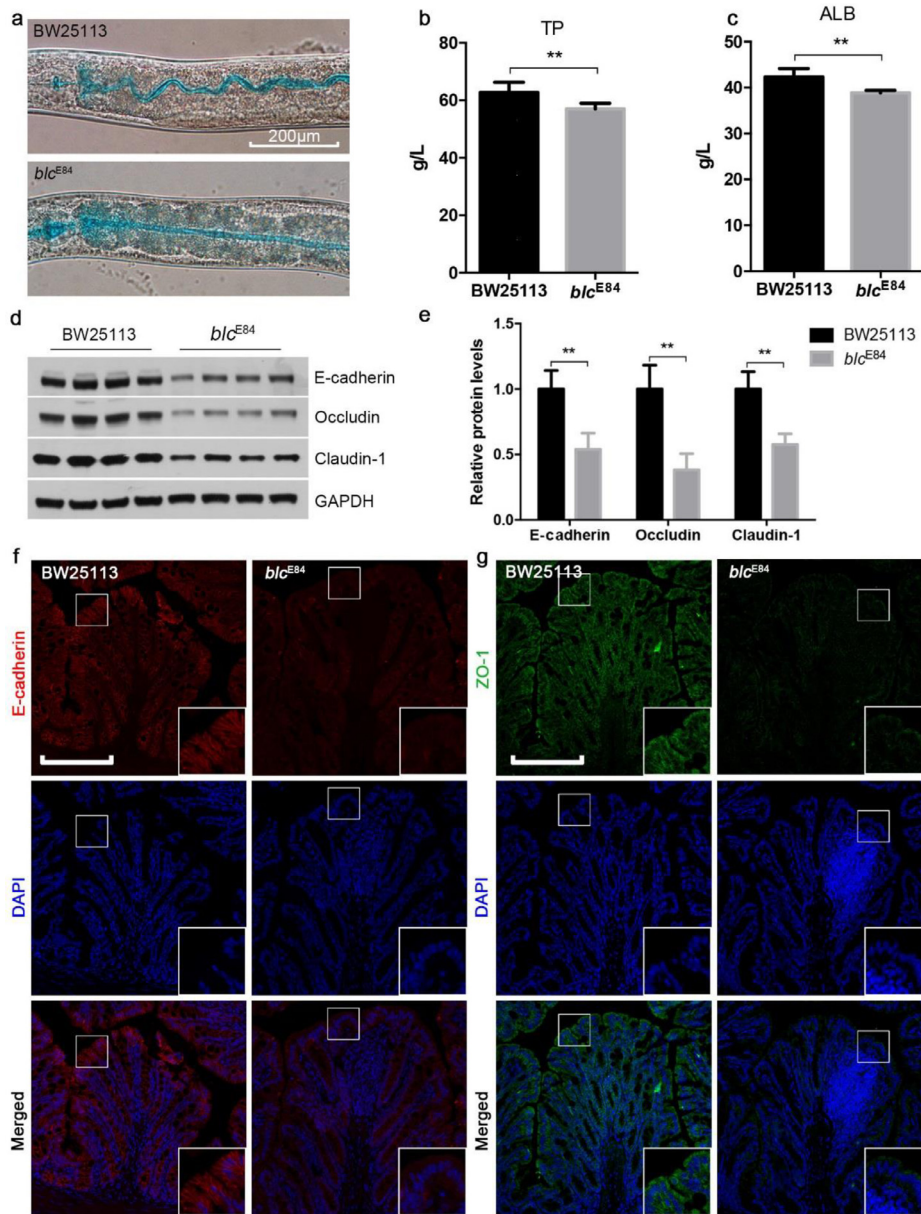
Fig. 3. *E. coli blc*[E84] disrupts the host intestinal epithelial barrier. (a) FD&C Blue No. 1 dye (erioglaucine disodium) staining of BW25113-treated and *E. coli blc*[E84]-treated worms. The scale bar represents 200 μm. (b−g) Male C57BL6/N AVNM mice were sacrificed on day 7 post-infection at the age of 9 weeks (*n* = 6). (b and c) Blood biochemical analysis of mouse serum total protein (TP) (b) and albumin (ALB) (c). Error bars represent the mean ± SD. **$p < 0.01$ (two-tailed Student's *t* test). (d and e) Western blots (d) and quantification (e) of the adherens junction (AJ) protein E-cadherin and the tight junction (TJ) proteins Occludin and Claudin-1 in the distal colons of infected mice. GAPDH served as the internal control. Error bars represent the mean ± SD. **$p < 0.01$ (two-tailed Student's *t* test). (f and g) Localization of the AJ protein E-cadherin (f) and TJ protein ZO-1 (g) in paraffin sections of the distal colon from BW25113-infected and *blc*[E84]-infected groups. (For interpretation of the references to color in this figure legend, the reader is referred to the web version of this article.)

data demonstrate that *E. coli blc*[E84] induces intestinal epithelial barrier disruption in both *C. elegans* and mice.

3.5. Epithelial barrier disruption precedes intestinal inflammation upon *E. coli blc*[E84] infection

The *E. coli blc*[E84]-infected mice showed two characteristics resembling the clinical symptoms of patients with IBD: upregulated inflammation and disrupted intestinal barrier integrity. Clarifying the time courses of these two phenotypes is important for dissecting the pathological consequences following *E. coli blc*[E84] infection. We examined mice infected with *E. coli blc*[E84] or BW25113 on day 1, 2, 3 and 5 post-infection. On day 1 post-infection, the level of Claudin-1 significantly decreased in the *E. coli blc*[E84]-infected mice, whereas E-cadherin and

Occludin remained comparable between the *E. coli blc*[E84]-infected and BW25113-infected mice (Fig. 4a and b). Meanwhile, the numbers of mature colonic goblet cells which are important for mucus, were significantly downregulated in the *E. coli blc*[E84]-infected mice (Fig. S7). To test the leakage of the intestine, FITC-dextran in PBS was introduced to infected mice by enema 2 h before blood collection. We found that the serum FITC level in *E. coli blc*[E84]-infected mice was significantly higher than that of the BW25113 group on day 1 post-infection (Fig. 4c). Consistently, we found that, compared to the BW25113-infected group, the *E. coli blc*[E84]-infected germ-free mice displayed increased bacterial burden in the whole blood, spleen and intestine-draining mesenteric lymph nodes (LNs). However, there were no differences in the bacterial burden in the liver between the two groups (Fig. 4d). After day 2 post-infection, the AJ protein E-cadherin and the TJ proteins Occludin
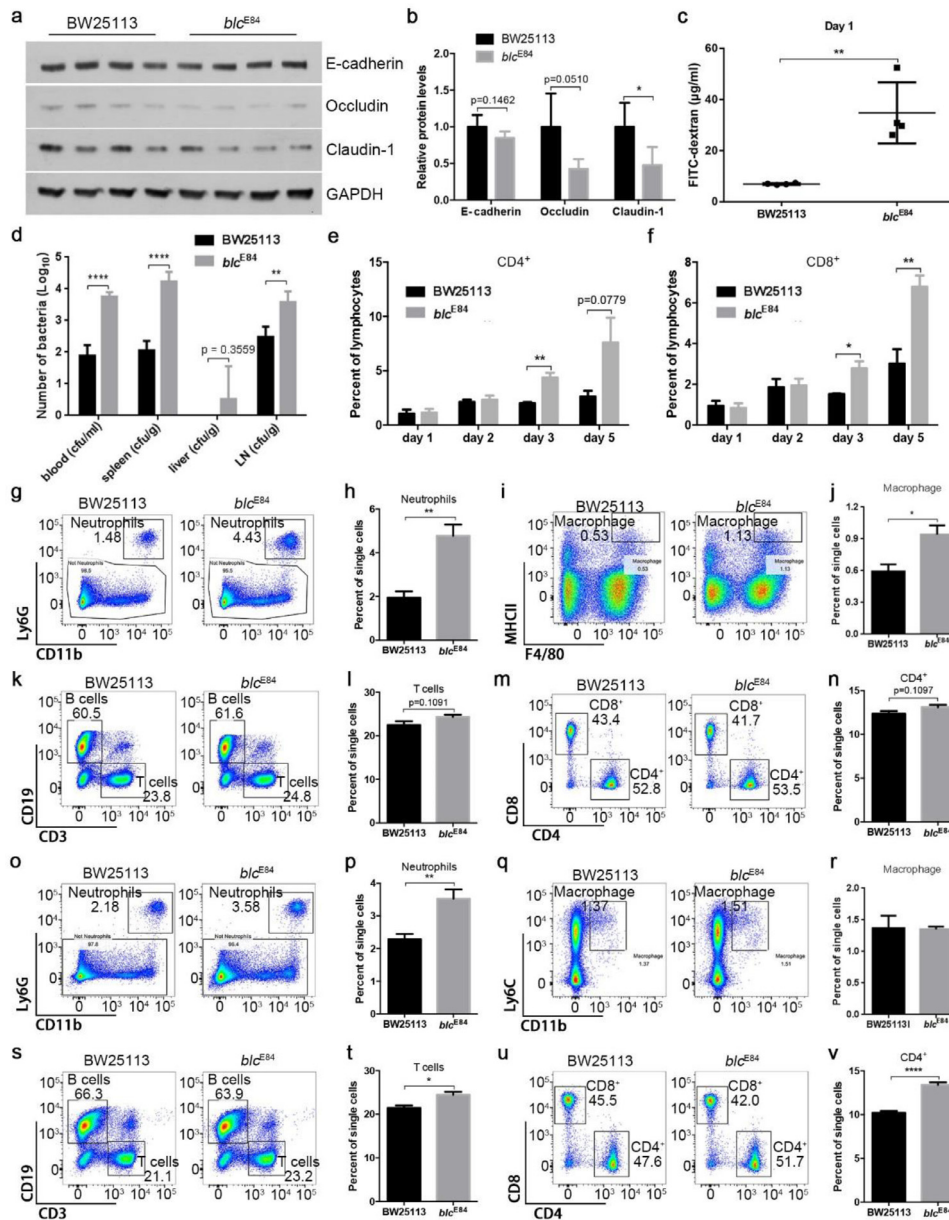
Fig. 4. *E. coli blc*^{E84} infection induces host intestinal epithelial barrier damage prior to the host immune response. (a and b) Western blots (a) and quantification (b) of E-cadherin, Occludin and Claudin-1 in the distal colons of BW25113 and *blc*^{E84} gavaged mice on day 1 post-infection. GAPDH served as the internal control. Error bars represent the mean ± SD (n = 4). *p < 0.05 (two-tailed Student's t test). (c) Assessment of intestinal permeability with enema FITC-dextran on day 1 post-infection. Error bars represent the mean ± SD. **p < 0.01 (two-tailed Student's t test). (d) Germ-free male mice at 10 weeks old were orally gavaged with a single inoculum of *E. coli* BW25113 or *E. coli blc*^{E84}. The number of CFUs on day 1 post-infection was determined in whole blood, spleen, liver and intestine-draining mesenteric lymph nodes (LNs) (n = 5). Error bars represent the mean ± SD. **p < 0.01, ****p < 0.0001 (two-tailed Student's t test). (e and f) Time course of CD4$^+$ (e) and CD8$^+$ (f) T cells in whole distal colon tissues from days 1 to 5 post-infection (n = 4). Error bars represent the mean ± SD. *p < 0.05, **p < 0.01 (two-tailed Student's t test). (g−n) Dot plots and quantification of neutrophils (g and h), macrophages (i and j), T cells (k and l) and CD4$^+$ T cells (m and n) in the spleens of infected mice on day 3 post-infection. Error bars represent the mean ± SEM (n = 4). *p < 0.05, **p < 0.01 (two-tailed Student's t test). (o−v) Dot plots and quantification of neutrophils (o and p), macrophages (q and r), T cells (s and t) and CD4$^+$ T cells (u and v) in the spleens of infected mice on day 5 post-infection. Error bars represent the mean ± SEM (n = 4). *p < 0.05, **p < 0.01, ****p < 0.0001 (two-tailed Student's t test).

and Claudin-1 in the colons of the *E. coli blc*^{E84}-infected mice all showed marked decreases compared to those in the BW25113 group (Fig. S8). These data indicate that infection with *E. coli blc*^{E84} induced colon epithelial barrier disruption in mice as early as 1 day after bacterial infection.

When we investigated the time course of inflammation activation, we found that only TNF-α was slightly upregulated in the colons of *E. coli blc*^{E84}-infected mice compared to the BW25113-infected group on day 1 and day 2 post-infection (Fig. S9a−f). This TNF-α increase may be due to the faster growth of *E. coli blc*^{E84} *in vivo*. When mice were infected with a single inoculum of a 1:10 (10^7 cfu:10^8 cfu), 1:1 (10^7 cfu:10^7 cfu), or 10:1 (10^8 cfu:10^7 cfu) mixture of *E. coli* BW25113

and *E. coli blc*^{E84}, we noticed higher *E. coli blc*^{E84} abundance in the gut than *E. coli* BW25113 after 24 h (Fig. S10a). However, the abundance of *E. coli blc*^{E84} in the gut decreased 3 days post-infection, which may be a consequence of immune activation (Fig. S10b). Indeed, two days after infection, inflammatory cytokines, including TNF-α, IL-1β, IL-4, IL-6, IL-8, and IL-17, and antimicrobial peptides, including the Reg3γ and Cryptdin families, were all significantly upregulated in the colons of *E. coli blc*^{E84}-infected mice compared to the BW25113 group (Fig. S9g−l). Consistently, we found that the proportions of CD4$^+$ T cells and CD8$^+$ T cells in colon tissue of the *E. coli blc*^{E84}-infected mice exhibited no difference from those of the BW25113 group until day 3 post-infection (Fig. 4e and f).

At the systemic level, the numbers of immunocytes, including neutrophils, monocytes, eosinophils, macrophages, CD4^{+} T cells, CD8^{+} T cells and NK cells, from the spleen and whole blood showed no differences between the two groups on day 1 and day 2 post-infection (Figs. S11 and S12 and Table S4). However, innate immunity-related immunocytes (Figs. 4g–j, S13a–d and S13i–p), including neutrophils (Fig. 4g and h), macrophages (Fig. 4i and j), and eosinophils (Fig. S13a and b) in the spleen, as well as neutrophils (Fig. S13i and j) and macrophages (Fig. S13o and p) in the blood, were significantly increased in the *E. coli blc*[E84]-infected mice compared to those in the BW25113 group on day 3 post-infection. The CD4^{+} T cell number was significantly increased in the whole blood from the *E. coli blc*[E84]-infected mice (Fig. S13s and t), while other adaptive immunity-related immunocytes in the spleen and whole blood remained unchanged on day 3 post-infection (Figs. 4k–n and S13e–h and q–w). On day 5 post-infection, adaptive immunity-related immunocytes at the local level (Fig. 4e and f) and the systemic level (Figs. 4s–v and S14e–h and q–w) were significantly increased, while some types of innate immunity-related immunocytes expanded (Figs. 4o and p and S14k and l) and others did not (Figs. 4q and r and S14a–d, i and j). All of the statistical results of absolute cell counts by flow cytometry are shown in Table S4. These data confirmed the result that the infection of *E. coli blc*E84 leads to immunocyte expansion at the systemic level at approximately day 3 post-infection. Moreover, we examined the ability of *E. coli blc*[E84] and BW25113 to activate activating innate immunity *in vitro*, and the data indicated no difference between the two strains (Fig. S15). These results suggest that *E. coli blc*[E84] infection stimulated the innate immune response on day 3 post-infection, followed by activated adaptive immunity. All the data above indicate that colonic enterocyte junction disruption occurred prior to the activation of local and systemic inflammation in *E. coli blc*[E84] infected mice.

3.6. Blc[E84] shows decreased binding affinity with LPE and causes decreased LPE concentration in E. coli

Next we asked how Blc[E84] triggered the immunological response. The biological function of the Blc[G84] protein, as reported, is to bind lysophospholipids (LPPs), especially lysophosphatidylethanolamine (LPE), as a dimer [36]. Lysophosphatidic acid (LPA), which is easily converted *in vivo* from LPE, plays an important role in alleviating bacteria-induced host diarrhea [28]. Thus, we hypothesized that Blc[E84] and Blc[E84] might display different dimerization or binding abilities to LPE.

The dimerization of Blc was analyzed by modified SDS-PAGE and liquid chromatography-mass spectrometry (LC-MS). The modified SDS-PAGE results showed that a band migrating near 37 kDa corresponded to the expected Blc[G84] and Blc[E84] dimers (Fig. 5b). The results were confirmed by LC-MS: Blc[G84] and Blc[E84] existed both as monomers (18,317 Da for Blc[G84] and 18,389 Da for Blc[E84]) and as dimers (36,633 Da for Blc[G84] and 36,777 Da for Blc[E84]) under non-denaturing conditions (Figs. 5a and S16). The difference between the molecular weight of glycine and glutamic acid is approximately 72 Da, and 72 Da was the difference between the Blc[G84] monomer and the Blc[E84] monomer, while the difference was 144 Da between the dimers. These results indicate that there is no difference between Blc[G84] and Blc[E84] dimerization under non-reducing conditions.

To examine the lipid binding of Blc[G84] and Blc[E84], we mixed prokaryotic-expressed and purified proteins with total lipids extracted from *E. coli Δblc*, and then the specific lipids bound by Blc[G84] or Blc[E84] were pulled down and identified by LC-MS. We found that Blc[G84] immunoprecipitated a greater variety of lipids than Blc[E84] (Fig. 5c). Blc[G84] showed higher lipid binding ability than Blc[E84], especially for LPE 16:0 and LPE 18:1 (Fig. 5d–f). These results indicate that Blc[E84], with its changed spatial structure, displays lower binding affinity to LPE.

This binding affinity change may be related to alternation of the protein structure. For Blc[G84], the glycine at the 84th position is located in a loop domain that links two beta-sheets [47]. Using SWISS-MODEL to model the Blc tertiary and quaternary structures [31], we found that the switch from an uncharged glycine to a negatively charged glutamic acid at Blc[E84] can attract the positively charged arginine at position 52 closer to the 84th position (Fig. 5g). This structural change may prevent the access of LPE binding because the arginine at position 52 is located at the entrance of the hydrophobic pocket of Blc, which is suited to bind lipid molecules. Therefore, the Blc G84E mutation may change the tertiary structure of Blc and influence its lipid binding ability.

Several studies have proposed that Blc helps bacteria as a retention machine for lipids [36,47]. To explore the lipid-bound profile with *E. coli blc*[E84] or *E. coli blc*[G84]. The total lipids were extracted from the bacterial cells and bacterial culture supernatant, and then identified by LC-MS. The results showed that both LPE and LPA were undetectable in the culture supernatant (Fig. S17), and *E. coli* BW25113 possessed more LPE 16:0 and LPE 18:1 in the cell than *E. coli blc*[E84] (Fig. 5h–j). These results suggest that these molecules may not be secreted but may be released by lytic *E. coli* cells.

3.7. LPE 18:1 rescues barrier disruption in the colonic epithelium of E. coli blc[E84]-infected mice

Our data showed decreased LPE storage in *E. coli blc*[E84]. To test whether *E. coli* BW25113 supplied more LPE to the host than *E. coli blc*[E84], faecal samples of mice on day 1 post-infection were collected and analyzed by LC-MS. Indeed, we found that faecal samples from *E. coli blc*[E84]-infected mice contained significantly less LPE 18:1 (Fig. 6c). The LPE 16:0 (Fig. 6a) and LPE 16:1 (Fig. 6b) levels showed slight decreases but no significant differences between the two groups. More importantly, these changes in intestinal lipid levels were also observed in faecal samples from patients with IBD. We found that LPE 16:0 (Fig. 6d) and LPE 18:1 (Fig. 6f) levels in faecal samples from patients with IBD were significantly decreased compared with those from healthy controls, whereas the LPE 16:1 (Fig. 6e) levels were comparable. However, the decrease in LPE tended to be a symptom of UC patients rather than CD patients (Fig. S3b–d). These results demonstrate that gut inflammation is associated with specific changes in gut LPE levels.

Finally, we examined whether LPE supplements could rescue *E. coli blc*[E84]-induced phenotypes in mice. LPE 18:1, which dissolved in peanut oil, was fed orally to AVNM mice on day 0. As expected, LPE-treated *E. coli blc*[E84]-infected mice displayed lower FITC in serum, compared to vehicle-treated *E. coli blc*[E84]-infected mice in the FITC-dextran assay on day 2 post-infection (Fig. 6g). This result indicates that LPE at 20 μM (200 μL per mouse) rescued the intestinal permeability defects induced by *E. coli blc*[E84] infection. Moreover, compared to the vehicle-fed *E. coli blc*[E84] infection group, colon tissue from mice in the LPE-treated *E. coli blc*[E84] infection group exhibited normal expression patterns and distributions of ZO-1, Occludin, and Claudin-1 (Figs. 6h–j and S18), suggesting the partial recovery of host intestinal permeability through reversing the downregulated and abnormally distributed junction proteins. In summary, *E. coli blc*[E84]-induced host colon epithelial barrier disruption was rescued by LPE supplementation, suggesting that the different phenotypes caused by *E. coli* BW25113 and *blc*[E84] infection in mice might be due to changed LPE supplements.

3.8. LPE activates the LPA1/PLCβ2/PKC axis to protect colon epithelial barrier function

Our data demonstrate that LPE supplementation could rescue *E. coli blc*[E84] infection-induced host colon epithelial barrier disruption *in vivo*. Previous reports have speculated that LPE could
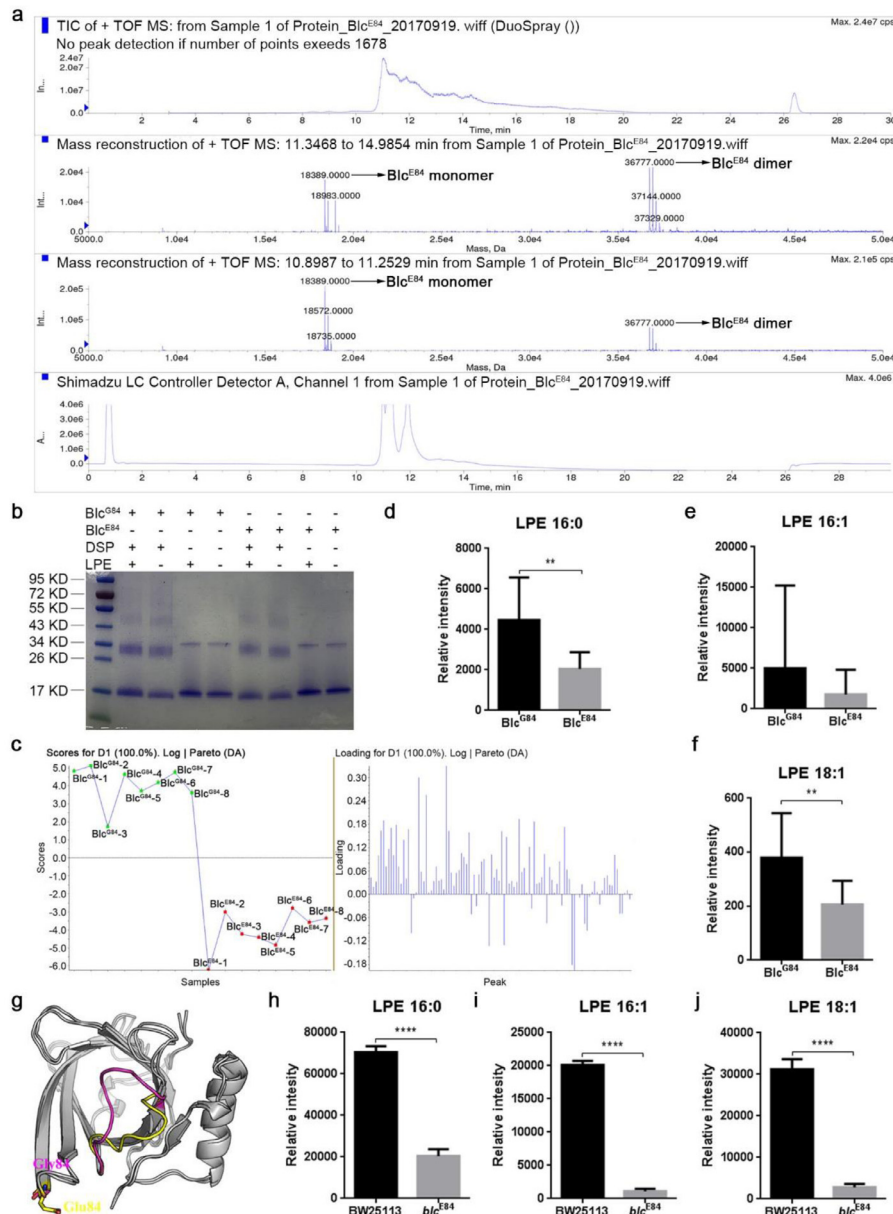
Fig. 5. Blc^{E84} spontaneously dimerized and downregulated the binding affinity with LPE. (a) LC-MS/MS spectra of the Blc^{E84} dimer. (b) Purified Blc^{G84} and Blc^{E84} protein, dissolved under non-reducing conditions, run in a modified SDS-PAGE with Coomassie blue staining. (c) Principal component analysis (PCA) of the lipids identified by LC/MS, which are represented by a vertical line (left panel), that were immunoprecipitated with purified Blc^{G84} and Blc^{E84} from the total lipids of *E. coli* Δblc (n = 6). (d–f) Lipid pull-down analysis of LPE 16:0 (d), 16:1 (e) and 18:1 (f) that were immunoprecipitated with purified Blc^{G84} and Blc^{E84} and identified by LC/MS (LPE 16:0, n = 8; LPE 16:1, n = 8; LPE 18:1, n = 7). Error bars represent the mean $\pm$ SD. **$p < 0.01$ (two-tailed Student's t test). (g) Alignment of the predicted structures of Blc^{G84} and Blc^{E84}. The conformational differences are highlighted in magenta (Blc^{G84}) and yellow (Blc^{E84}). (h–j) Lipid conformation analysis of LPE 16:0 (h), 16:1 (i) and 18:1 (j) that were extracted from *E. coli* cells and identified by LC/MS (n = 8). Error bars represent the mean $\pm$ SD. **$p < 0.01$, ****$p < 0.0001$ (two-tailed Student's t test). (For interpretation of the references to color in this figure legend, the reader is referred to the web version of this article.)

activate LPA$_1$ signaling, which functions to sustain endothelial and epithelial barrier integrity [48,49]. We then tested whether a similar pathway was involved the *E. coli blc*^{E84} infection-induced host colon epithelial barrier. In the cell culture model, LPA treatment upregulate TJ and AJ proteins and enhanced the barrier function of Caco-2 monolayers [50]. Our data showed that LPE could reverse H$_2$O$_2$-induced downregulation of TJ and AJ proteins in a dose-dependent manner [51] (Fig. 7a and b). As expected, pre-treatment with two LPA$_1$ antagonists, AM095 and Ki16425, blocked the protective function of LPE (Fig. 7c and d). LPA is the product of LPE and a stronger agonist of LPA$_1$ than LPE (Fig. 7a and b). To exclude the possibility that the protective function of LPE relied on its transformation into LPA, two autotaxin (ATX) inhibitors, HA130 and

GLPG1690, were used. The results showed that HA130 and GLPG1690 could not inhibit LPE-induced upregulation of TJ and AJ proteins (Fig. S19). These data indicate that the protective function of LPE is directly via LPA$_1$.

To test the *in vivo* function of the LPA$_1$ receptor in the gut, the LPA$_1$ inhibitor Ki16425 was injected i.p. into mice before *E. coli* BW25113 or *blc*^{E84} infection. The FITC-dextran assay showed that *E. coli* BW25113 caused damage to the intestinal barrier of the mouse after the LPA$_1$ signaling of the host was blocked (Fig. 7e), suggesting that LPE protects the epithelial barrier through LPA$_1$.

Since LPA is the product of LPE, and its efficiency in activating LPA$_1$ is higher than that of LPE, we explored whether intestinal barrier integrity benefits from the transformation from LPE to LPA. Our
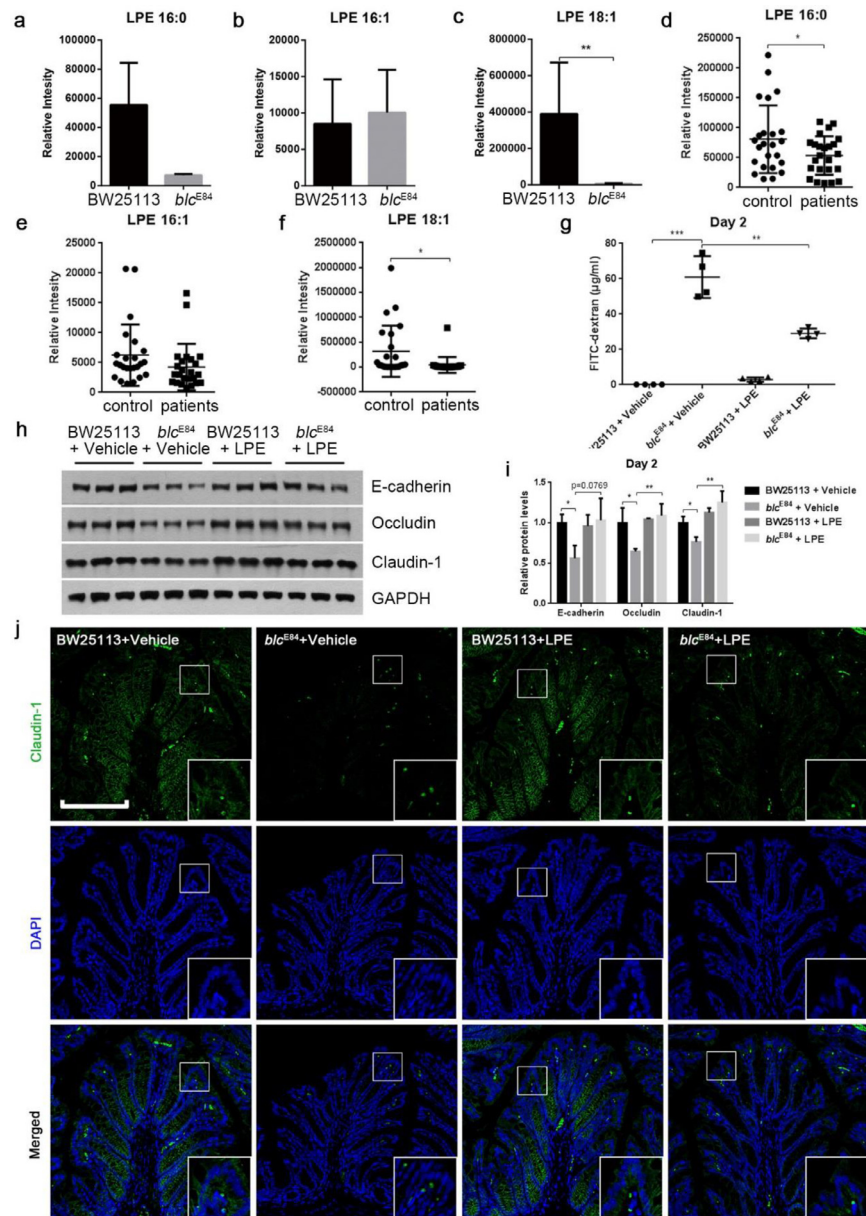
Fig. 6. LPE 18:1 rescues *E. coli* blc^{E84} infection-induced host intestinal barrier disruption. AVNM-treated male B6N mice at 8 weeks old were gavaged with *E. coli* culture (10^8 cfu) once followed by LPA oral administration. Mice were sacrificed on day 2 post-infection ($n = 4$). (a−c) LC/MS/MS spectra of LPE 16:0 (a), LPE 16:1 (b) and LPE 18:1 (c) from mouse faecal samples. Error bars represent the mean ± SD ($n = 8$). $**p < 0.01$ (two-tailed Student's *t* test). (d−f) LC/MS/MS spectra of LPE 16:0 (d), LPE 16:1 (e) and LPE 18:1 (f) from faeces from healthy people and patients with IBD (control = 24; patients = 24). Error bars represent the mean ± SEM. $*p < 0.05$ (two-tailed Student's *t* test). (g) Assessment of the intestinal permeability of LPE-treated, vehicle-treated mice with enema FITC-dextran on day 2 post-infection. Error bars represent the mean ± SD ($n = 4$). $**p < 0.01$, $***p < 0.001$ (two-tailed Student's *t* test and p.adjust with Benjamini & Hochberg). (h and i) Western blots (h) and quantification (i) of the AJ protein E-cadherin and TJ proteins Occludin and Claudin-1 in the colons of infected mice. GAPDH served as the internal control. Error bars represent the mean ± SD ($n = 4$). $*p < 0.05$, $**p < 0.01$ (two-tailed Student's *t* test and p.adjust with Benjamini & Hochberg). (j) Localization of the TJ protein Claudin-1 in paraffin sections of the distal colon from all four groups.

ELISA results showed that the total LPA content in the faeces of the BW25113-infected mice was significantly higher than that in the blc^{E84}-infected group (Fig. S20). These data suggested that LPE supplementation by BW25113 could be the source of the LPA substrate. Therefore, we treated mice directly with LPA and then tested the response of the mice to the two bacterial infections. As expected, when LPA was administered, *E. coli* blc^{E84}-infected mice displayed lower FITC in serum compared to vehicle group on day 2 post-infection (Fig. 7f). Meanwhile, LPA treatment restored the expression pattern of TJ and AJ proteins (Figs. 7g and h, S21 and S22). In summary, *E. coli* blc^{E84}-induced host colon epithelial barrier disruption could be rescued by LPA supplementation, suggesting that the different phenotypes caused by *E. coli* BW25113 and blc^{E84} infection in mice might be the consequence of different LPA_1 activation.

PKC has been recognized to influence IEC signaling [52]. Several studies have suggested that LPA_1 activates protein kinase C (PKC) via a PLCβ-induced DAG increase. Our data showed that LPE and LPA treatment could increase PKC activity, with a phorbol ester (PMA)-treated group as the positive control (Fig. 7i). The pan-PKC inhibitor GF 109203X blocked LPE-induced TJ and AJ protein increases (Fig. 7j and k). To explore the function of PLCβ in LPA_1-induced PKC activation, siRNA was used to knockdown PLCβ1 and PLCβ2 (Fig. S23). We found that knockdown of PLC-β2 but not PLC-β1 ablated LPE-induced upregulation of TJ and AJ proteins (Fig. 7l and m). These
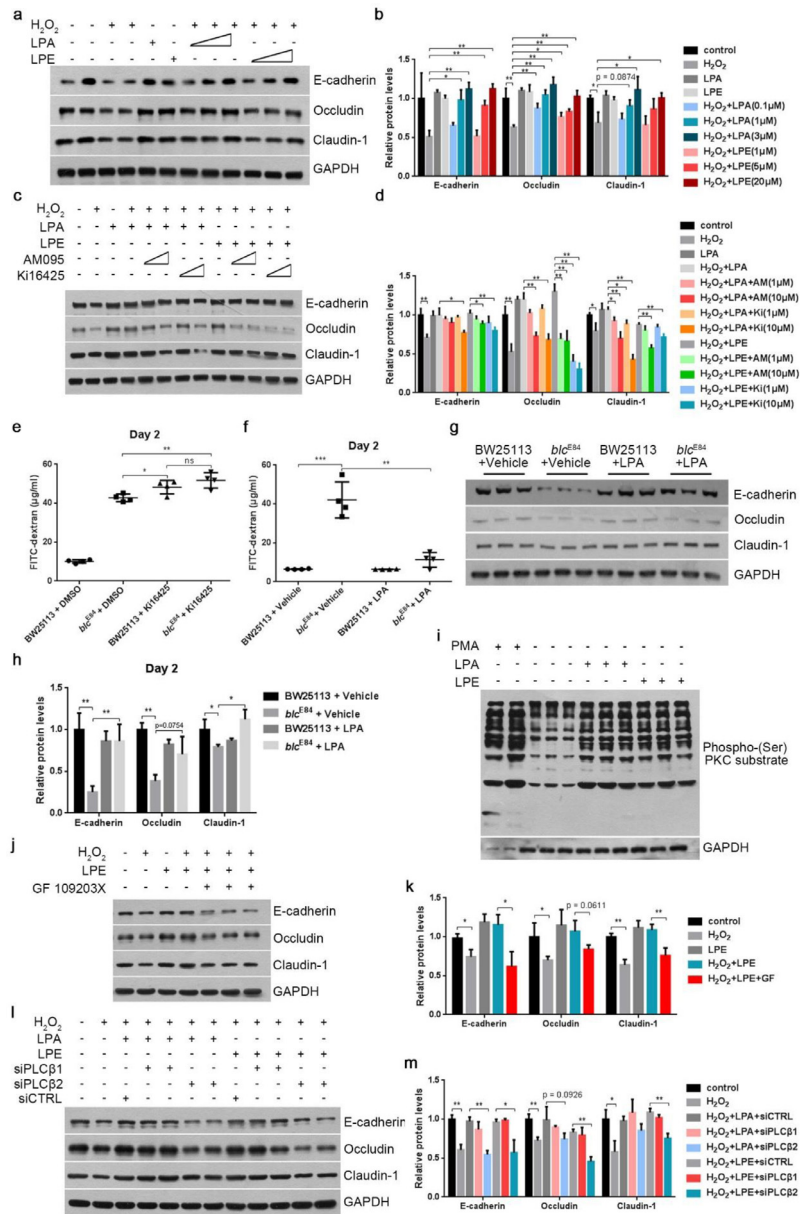
Fig. 7. LPE activates the LPA$_1$/PLCβ2/PKC axis to protect colon epithelial barrier function. (a and b) Western blots (a) and quantification (b) of E-cadherin, Occludin and Claudin-1 in Caco-2 cells treated with LPA (0.1 μM, 1 μM, 3 μM) or LPE (1 μM, 5 μM, 20 μM). GAPDH served as the internal control. Error bars represent the mean ± SD. (three biological replicates). $^*p < 0.05$, $^{**}p < 0.01$ (two-tailed Student's t test and p.adjust with Benjamini & Hochberg). (c and d) Western blots (c) and quantification (d) for E-cadherin, Occludin and Claudin-1 of AM095 (1 μM, 10 μM) or Ki16425 (1 μM, 10 μM) treated Caco-2 cells pre-treated with LPA (1 μM) or LPE (20 μM). GAPDH served as the internal control. Error bars represent the mean ± SD. (three biological replicates). $^*p < 0.05$, $^{**}p < 0.01$ (two-tailed Student's t test and p.adjust with Benjamini & Hochberg). (e) Assessment of the intestinal permeability of Ki16425-i.p. injected (20 mg/kg) and DMSO-i.p. injected mice with enema FITC-dextran on day 2 post-infection ($n = 4$). Error bars represent the mean ± SD. $^*p < 0.05$, $^{**}p < 0.01$ (two-tailed Student's t test and p.adjust with Benjamini & Hochberg). (f) Assessment of the intestinal permeability of LPA-treated and vehicle-treated mice with enema FITC-dextran on day 2 post-infection ($n = 4$). Error bars represent the mean ± SD. $^{**}p < 0.01$, $^{***}p < 0.001$ (two-tailed Student's t test and p.adjust with Benjamini & Hochberg). (g and h) Western blots (g) and quantification (h) of the AJ protein E-cadherin and the TJ proteins Occludin and Claudin-1 in the colons of infected mice. GAPDH served as the internal control. Error bars represent the mean ± SD. $^*p < 0.05$, $^{**}p < 0.01$ (two-tailed Student's t test and p.adjust with Benjamini & Hochberg). (i) Western blots for the phospho-(Ser) PKC substrate of LPA (1 μM) or LPE (20 μM)-treated Caco-2 cells. Caco-2 cells were treated with PMA (1 μM) for 0.5 h (lane 1) and 4 h (lane 2) as the positive controls. GAPDH served as the internal control. (j and k) Western blots (j) and quantification (k) of E-cadherin, Occludin and Claudin-1 of shPLCβ1- or shPLCβ2-treated Caco-2 cells. Error bars represent the mean ± SD. (three biological replicates). $^*p < 0.05$, $^{**}p < 0.01$ (two-tailed Student's t test and p.adjust with Benjamini & Hochberg). (l and m) Western blots (l) and quantification (m) of E-cadherin, Occludin and Claudin-1 in Caco-2 cells treated with the pan-PKC inhibitor GF-109203X (10 μM). GAPDH served as the internal control. Error bars represent the mean ± SD. (three biological replicates). $^*p < 0.05$, $^{**}p < 0.01$ (two-tailed Student's t test and p.adjust with Benjamini & Hochberg).

results indicate that LPE-induced enhancement of epithelial barrier integrity depends on the LPA$_1$/PLCβ2/PKC axis.

4. Discussion

We demonstrate here that the *E. coli*-encoded *blc* gene can affect host intestinal barrier integrity and immunological homeostasis,

while pathogenic *E. coli* usually carry a SNP in *blc* that results in a single amino acid change from Blc^{G84} to Blc^{E84}. Mice infected with bacteria expressing Blc^{E84} display a diarrheal phenotype along with defective epithelial permeability. Moreover, *E. coli* blc^{E84} is significantly enriched in patients with IBD, which may provide a new biomarker for diagnosis. Our study identifies a variant in chromosomal bacterial genes that is irrelevant to virulence and can severely affect

the host intestinal barrier, suggesting that a single genome or gene expression level can play a significant role in the host-microbiome/pathogen interaction.

As the Table S1 showed, the ratios of two *blc* SNP variants are comparable at the species level. However, the Blc^{E84} variant was conserved in most clear-identified pathogenic *E. coli*, compared to the commensal non-pathogenic strains (Fig. 1e and f). Based on our study, the Blc^{E84} variant might represent an important new pathogenic mechanism in *E. coli* in addition to LPS. It worths to characterize the pathogenic ability of all the sequenced *E. coli*.

An injured intestinal epithelium with inflammation may create a hyperoxic microenvironment in the gut, giving a slight growth advantage to facultatively anaerobic bacteria over anaerobic bacteria [5]. Patients with IBD have an increased relative abundance of Enterobacteriaceae, especially *E. coli*, in the terminal ileum and rectum, and this increase is strongly correlated with the disease process [53]. AIEC strains such as NRG 857C and LF82, which were reported to contribute to the progression of CD, also contain the g251a (G84E) SNP site [41,42]. This phenomenon shows that non-pathogenic *E. coli* is less competitive in the inflammatory microenvironment, which is in line with a recent report [54]. We also found that the ratio of *blc*^{E84}/*blc*^{G84} was significantly upregulated in IBD patient samples and in co-infected mice (Figs. 1g and S10), which indicates that pathogenic *E. coli blc*^{E84} displays a growth advantage in the inflamed intestine. However, *blc*^{a251}/Blc^{E84} variant cannot explain all pathogenic *E. coli*-caused host pathogenesis: first, this variant is not possessed by all pathogenic *E. coli* serotypes (Fig. 1e and Table S1); second, pathogenic *E. coli* has other effector proteins and toxins, such as the type 3 secretion system and Shiga toxin. To explore the association between decreased *blc*^{E84}/*blc*^{G84} ratio and disease activity index, the medical history, phase of the disease, more samples are required for further investigations.

The paternal *E. coli* strain BW25113 belongs to a clear lineage of K-12 *E. coli*. This strain does not possess any key PAIs that enable bacteria or bacterial metabolites to cross the host intestinal barrier [25]. Hence, the *blc* g251a knock-in *E. coli blc*E84 strain, which was based on *E. coli* BW25113, lacked the ability to pass through the colon epithelium unless the barrier was disrupted. In our *E. coli*-infected AVNM pre-treated mouse model, the residual endogenous microbes after antibiotic treatment may be a key reason to explain why *E. coli* blc^{E84} caused a host immune response in mice after infection. Perhaps after *E. coli* blc^{E84} infection, disruption of the intestinal barrier occurs first, but the subsequent invasion of other bacteria (opportunistic pathogens) leads to an increase in systemic inflammation. Our data in Fig. S6 show that the *E. coli* blc^{E84}-infected GF mice displayed increased bacterial burden, which, however, could not prove the enhanced invasion of *E. coli* blc^{E84} compared to BW25113. This phenomenon might be the consequence of a disrupted epithelial barrier at an early stage. This was consistent with the result that mice infected with *E. coli* carrying *blc*E84 showed colonic barrier disruption prior to increased inflammation in our study. The cell junction-related protein Claudin-2 responded quickly to *C. rodentium* infection, as early as 2 days after infection [55]. Our data showed that the TJ and AJ proteins in colonic enterocytes were downregulated as early as 1 day after infection. In previous studies, systemic inflammation began to develop 3 days after infection with the murine-specific pathogen *Citrobacter rodentium* and the pathobiont *P. mirabilis* [5,56]. In this study, the *E. coli blc*E84-infected mice also showed a detectable antimicrobial response on day 3 post-infection (Figs. S9−S14). At the systemic level, innate immunity-related immunocytes were upregulated on day 3 post-infection. The adaptive immunity-related immunocytes increased on day 5 post-infection (Figs. 4 and S14), except that the CD4+ T cell number showed significant upregulation on day 3 post-infection (Fig. S13t). Moreover, we found that the downregulated abundance of *E. coli* blc^{E84} on day 3 post-infection displayed a negative correlation with host immune activation (Figs. S10b, 4e−n,

S9g−I and S13). However, the abnormal immune system of patients with IBD may cause intestinal dysbiosis and impaired *E. coli* blc^{E84} clearance, which could promote the development of the disease. These results suggest that, for many species of pathogenic bacteria, including BlcE84-containing E. coli, disruption of the host intestinal epithelial barrier might be necessary for intestinal inflammation.

A multiomics-based study showed a significant decrease in LPE in faeces of CD and UC patients [53]. However, we mechanically explained the correlation between two related phenotypes of IBD: 1. *E. coli* increase; 2. LPE decrease. Our study revealed that the decreased binding capacity between the *E. coli* Blc^{E84} protein and LPE caused the downregulation of LPE in both the bacterial cell and the host lumen.

The physiological function of Blc is not fully understood. The crystal structure and biochemical study demonstrated that the Blc^{G84} protein forms a dimer and may store bacterial lipids with a binding preference for lysophospholipids (LPPs) [36]. The replacement of an uncharged glycine by a negatively charged glutamic acid in Blc^{E84} may attract the positively charged arginine at position 52 to the glutamic acid at position 84 by computer simulation (Fig. 5g). This structural change may affect the binding affinity for LPE because the arginine at position 52 is located at the entrance to the hydrophobic pocket of Blc for LPE binding [36]. Indeed, we found that Blc^{E84} displays much lower affinity for LPE than Blc^{G84} (Fig. 5c−f). *E. coli* BW25113, which encodes Blc^{G84}, stores more LPE than *E. coli* blc^{E84} (Figs. 5h−j and S17). Based on our studies, we speculated that *E. coli* may not secrete LPA and LPE, but these molecules might be released into the host intestine from dead bacteria (Fig. S17). Consistent with this, non-pathogenic bacteria encoding Blc^{G84} helped to maintain intestinal LPE18:1 and LPE16:0 levels, whereas infection with the pathogenic bacteria containing Blc^{E84} resulted in lower levels of these two lysophospholipids in both mice and humans (Fig. 6a−f).

Previous studies have suggested that lysophospholipids are crucial for regulating epithelial integrity and physiological homeostasis. As the key product of LPPs, LPA relieves intestinal inflammation by increasing salt absorption and decreasing anion secretion [57]. LPA can maintain intestinal ion homeostasis by mediating the function of Na$^+$/H$^+$ exchanger 3 (NHE3) [28], cystic fibrosis transmembrane conductance regulator (CFTR) [58] and Cl$^-$/OH$^-$ exchanger through the LPA receptor [59]. Consistent with these functions, LPA receptor 1 knockout mice (*lpa1*$^{-/-}$) showed increased intestinal barrier permeability and downregulated TJ and AJ protein expression in the colon [50]. Bone marrow-derived dendritic cells (BM-DCs) from LPA receptor 2 knockout mice (*lpa2*$^{-/-}$) showed dramatically downregulated IL-10 secretion and upregulated TNF-α production under lipopolysaccharide (LPS) stimulation [60]. However, in this study, supplementation with LPE 18:1 reversed the detrimental effects of *blc*^{E84} bacteria-infected mice, and the LPA$_1$ signaling axis was activated during LPE treatment (Figs. 6g−j, S18, 7a−d and S21). These data verify the prediction in previous reports that LPE can activate LPA$_1$ [48]. In this study, we found that in a mouse model, both LPA and LPE could rescue the phenotype of *E. coli* blc^{E84} infection. Although we demonstrate that LPE can activate LPA$_1$ directly, the efficacy is lower than that of LPA. In the physical environment, LPE released from commensal microbiota could either activate the LPA$_1$ pathway directly, or be transformed to LPA by ATX at first and then activate the LPA$_1$ pathway. For future clinical trials, the combination of LPE, LPA and other related lysophospholipids may be more efficient than single lipids.

Activated LPA signaling mediates the function of protein kinase C [61]. We showed that LPE stimulated PKC activation and that a pan-inhibitor of PKC could block the protective functions of LPE. Classical PKC (cPKC) (α, β and γ) and novel PKC (nPKC) isotypes (δ, ε, η and θ) have been reported to trigger the translocation of TJ and AJ proteins to the cell membrane [62]. This is consistent with our results that activated PKC signalling via PLCβ2 could protect Caco-2 cells from oxidative damage. Moreover, previous studies have demonstrated

that the PKC agonist PMA is capable of inducing TJ fibrils in MDCK cells [62]. In addition, the participation of PKCs in TJ disassembly has been studied in different systems, and complicated PKC signaling to epithelial cell junctions has been demonstrated [52]. A direct interaction of ERK, which is downstream of activated PKC, with the C-terminal region of Occludin has been reported, and this interaction helps to maintain the stability and localization of TJ proteins [63]. The H_2O_2-induced redistribution of TJ and AJ proteins and the increase in barrier permeability were reversed by inhibiting the activity of PP2A [64]. As a Ser/Thr phosphatase, PP2A is functionally antagonistic to PKC which has serine/threonine kinase activity. Additionally, some studies have shown that the MEK/ERK MAPK signalling pathway is crucial in PKC activation-mediated Caco-2 resistance to oxidative stress [63]. These studies indicate that the activation of PKC plays an important role in sustaining colon epithelial cell junctions. However, which of the three PKC isotypes participate in LPE-mediated barrier protection requires further study.

Our study indicates that the blc^{a251} variant could be used as an indicator for the diagnosis of inflammatory bowel disease, and could be helpful for the classification of inflammatory bowel disease subtypes to facilitate targeted treatment. Moreover, lysophosphatidylethanolamine is widely found in foods including rice and wheat, so supplementation with lysophosphatidylethanolamine is safe and may also be helpful for the remission of inflammatory bowel disease.

In conclusion, our study reveals the novel functions of bacterial Blc in maintaining intestinal homeostasis. We also identified a pathogenic variant in patients with IBD. Our studies suggest a therapeutic application of LPE and LPA, suggesting that Blc^{G84} serves as a protective factor for host gut epithelial barrier integrity by increasing LPE storage. An in-depth study of this pathway may shed light on these novel pathogenic processes and provide new targets for the treatment of related diseases.

Declaration of competing interest

We declare no potential conflicts of interest concerning the research, authorship, and/or publication of this article, except a patent that we have (Number: 201911273194.1).

Acknowledgments

Supplementary materials

Supplementary material associated with this article can be found in the online version at doi:10.1016/j.ebiom.2020.102652.

References

[1] Izcue A, Coombes JL, Powrie F. Regulatory lymphocytes and intestinal inflammation. Ann Rev Immunol 2009;27:313–38.
[2] Arthur JC, Perez-Chanona E, Muhlbauer M, Tomkovich S, Uronis JM, Fan TJ, et al. Intestinal inflammation targets cancer-inducing activity of the microbiota. Science 2012;338(6103):120–3.
[3] Rangan KJ, Pedicord VA, Wang YC, Kim B, Lu Y, Shaham S, et al. A secreted bacterial peptidoglycan hydrolase enhances tolerance to enteric pathogens. Science 2016;353(6306):1434–7.
[4] Zhao L, Zhang F, Ding X, Wu G, Lam YY, Wang X, et al. Gut bacteria selectively promoted by dietary fibers alleviate type 2 diabetes. Science 2018;359(6380):1151–6.
[5] Lopez CA, Miller BM, Rivera-Chavez F, Velazquez EM, Byndloss MX, Chavez-Arroyo A, et al. Virulence factors enhance citrobacter rodentium expansion through aerobic respiration. Science 2016;353(6305):1249–53.
[6] Round JL, Mazmanian SK. The gut microbiota shapes intestinal immune responses during health and disease. Nat Rev Immunol 2009;9(5):313–23.
[7] Ivanov II, Atarashi K, Manel N, Brodie EL, Shima T, Karaoz U, et al. Induction of intestinal Th17 cells by segmented filamentous bacteria. Cell 2009;139(3):485–98.
[8] Morrison PJ, Bending D, Fouser LA, Wright JF, Stockinger B, Cooke A, et al. Th17-cell plasticity in helicobacter hepaticus-induced intestinal inflammation. Mucosal Immunol 2013;6(6):1143–56.
[9] Muehlbauer M, Gharaibeh RZ, Arthur JC, Fodor AA, Jobin C. 825 intestinal inflammation targets E. Coli NC101 transcriptome response and promotes development of colorectal cancer (CRC). Gastroenterology 2013;144(5):S-144–5.
[10] Hood MI, Skaar EP. Nutritional immunity: transition metals at the pathogen-host interface. Nat Rev Microbiol 2012;10(8):525–37.
[11] Nataro JP, Kaper JB. Diarrheagenic Escherichia coli. Clin Microbiol Rev 1998;11(1):142–201.
[12] Levy HL, Sepe SJ, Shih VE, Vawter GF, Klein JO. Sepsis due to Escherichia coli in neonates with galactosemia. N Engl J Med 1977;297(15):823–5.
[13] Johnson JR. Virulence factors in Escherichia coli urinary tract infection. Clin Microbiol Rev 1991;4(1):80–128.
[14] Glode MP, Sutton A, Robbins JB, McCracken GH, Gotschlich EC, Kaijser B, et al. Neonatal meningitis due of Escherichia coli K1. J Infect Dis 1977;136(Suppl):S93–7.
[15] Mortality GBD. Causes of death C. Global, regional, and national age-sex specific all-cause and cause-specific mortality for 240 causes of death, 1990-2013: a systematic analysis for the global burden of disease study 2013. Lancet 2015;385(9963):117–71.
[16] Tenaillon O, Skurnik D, Picard B, Denamur E. The population genetics of commensal Escherichia coli. Nat Rev Microbiol 2010;8(3):207–17.
[17] Mowat AM. Anatomical basis of tolerance and immunity to intestinal antigens. Nat Rev Immunol 2003;3(4):331–41.
[18] Hacker J, Kaper JB. Pathogenicity islands and the evolution of microbes. Annu Rev Microbiol 2000;54:641–79.
[19] Abreu MT, Vora P, Faure E, Thomas LS, Arnold ET, Arditi M. Decreased expression of Toll-like receptor-4 and MD-2 correlates with intestinal epithelial cell protection against dysregulated proinflammatory gene expression in response to bacterial lipopolysaccharide. J Immunol 2001;167(3):1609–16.
[20] Rembacken BJ, Snelling AM, Hawkey PM, Chalmers DM, Axon AT. Non-pathogenic Escherichia coli versus mesalazine for the treatment of ulcerative colitis: a randomised trial. Lancet 1999;354(9179):635–9.
[21] Magerl M, Lammel V, Siebenhaar F, Zuberbier T, Metz M, Maurer M. Non-pathogenic commensal Escherichia coli bacteria can inhibit degranulation of mast cells. Exp Dermatol 2008;17(5):427–35.
[22] Scott TA, Quintaneiro LM, Norvaisas P, Lui PP, Wilson MP, Leung KY, et al. Host-microbe co-metabolism dictates cancer drug efficacy in C. elegans. Cell 2017;169(3):442–56 e18.
[23] Garcia-Gonzalez AP, Ritter AD, Shrestha S, Andersen EC, Yilmaz LS, Walhout AJM. Bacterial metabolism affects the C. elegans response to cancer chemotherapeutics. Cell 2017;169(3):431–41 e8.
[24] Han B, Sivaramakrishnan P, Lin CJ, Neve IAA, He J, Tay LWR, et al. Microbial genetic composition tunes host longevity. Cell 2017;169(7):1249–62 e13.
[25] Baba T, Ara T, Hasegawa M, Takai Y, Okumura Y, Baba M, et al. Construction of Escherichia coli K-12 in-frame, single-gene knockout mutants: the Keio collection. Mol Syst Biol 2006;2:2006:0008.
[26] Tan M, Mahajanmiklos S, Ausubel FM. Killing of caenorhabditis elegans by pseudomonas aeruginosa used to model mammalian bacterial pathogenesis. Proc Natl Acad Sci U S A 1999;96(2):715–20.
[27] Ayres JS, Trinidad NJ, Vance RE. Lethal inflammasome activation by a multidrug-resistant pathobiont upon antibiotic disruption of the microbiota. Nat Med 2012;18(5):799–806.
[28] Lin S, Yeruva S, He P, Singh AK, Zhang H, Chen M, et al. Lysophosphatidic acid stimulates the intestinal brush border Na(+)/H(+) exchanger 3 and fluid absorption via LPA(5) and NHERF2. Gastroenterology 2010;138(2):649–58.
[29] Lee S, Leoni G, Neumann P, Chun J, Nusrat A, Yun CC. Distinct phospholipase C-β isozymes mediate lysophosphatidic acid receptor 1 effects on intestinal epithelial homeostasis and wound closure. Mol Cell Biol 2013;33(10):2016–28.
[30] Gibson DL, Ma C, Bergstrom KS, Huang JT, Man C, Vallance BA. MyD88 signalling plays a critical role in host defence by controlling pathogen burden and promoting epithelial cell homeostasis during Citrobacter rodentium-induced colitis. Cell Microbiol 2008;10(3):618–31.
[31] Biasini M, Bienert S, Waterhouse A, Arnold K, Studer G, Schmidt T, et al. SWISS-MODEL: modelling protein tertiary and quaternary structure using evolutionary information. Nucleic Acids Res 2014;42(Web Server issue):W252–8.
[32] Duan Y, Wu C, Chowdhury S, Lee MC, Xiong G, Zhang W, et al. A point-charge force field for molecular mechanics simulations of proteins based on condensed-phase quantum mechanical calculations. J Comput Chem 2003;24(16):1999–2012.
[33] Jorgensen WL, Chandrasekhar J, Madura JD, Impey R, Klein ML. Comparison of simple potential functions for simulating liquid water. J Chem Phys 1983;79(2):926–35.
[34] Darden T, York DM, Pedersen LG. Particle mesh Ewald: an N·log(N) method for Ewald sums in large systems. J Chem Phys 1993;98(12):10089–92.
[35] Ryckaert J, Ciccotti G, Berendsen HJC. Numerical integration of the cartesian equations of motion of a system with constraints: molecular dynamics of n-alkanes. J Comput Phys 1977;23(3):327–41.
[36] Campanacci V, Bishop RE, Blangy S, Tegoni M, Cambillau C. The membrane bound bacterial lipocalin Blc is a functional dimer with binding preference for lysophospholipids. FEBS Lett 2006;580(20):4877–83.
[37] Cai Z, Jitkaew S, Zhao J, Chiang HC, Choksi S, Liu J, et al. Plasma membrane translocation of trimerized MLKL protein is required for TNF-induced necroptosis. Nat Cell Biol 2014;16(1):55–65.

[38] Troemel ER, Chu SW, Reinke V, Lee SS, Ausubel FM, Kim DH. p38 MAPK regulates expression of immune response genes and contributes to longevity in C. elegans. PLoS Genet 2006;2(11):e183.

[39] Keseler IM, Collado-Vides J, Gama-Castro S, Ingraham J, Paley S, Paulsen IT, et al. EcoCyc: a comprehensive database resource for Escherichia coli. Nucleic Acids Res 2005;33(Database issue):D334–7.

[40] Lukjancenko O, Wassenaar TM, Ussery DW. Comparison of 61 sequenced Escherichia coli genomes. Microb Ecol 2010;60(4):708–20.

[41] Nash JHE, Villegas A, Kropinski AM, Aguilarvalenzuela R, Konczy P, Mascarenhas M, et al. Genome sequence of adherent-invasive Escherichia coli and comparative genomic analysis with other E. coli pathotypes. BMC Genom 2010;11(1):667.

[42] Carvalho FA, Barnich N, Sauvanet P, Darcha C, Gelot A, Darfeuillemichaud A. Crohn's disease-associated Escherichia coli LF82 aggravates colitis in injured mouse colon via signaling by flagellin. Inflamm Bowel Dis 2008;14(8):1051–60.

[43] Neurath MF. Cytokines in inflammatory bowel disease. Nat Rev Immunol 2014;14 (5):329–42.

[44] Gelino S, Chang JT, Kumsta C, She X, Davis A, Nguyen C, et al. Intestinal autophagy improves healthspan and longevity in C. elegans during dietary restriction. PLoS Genet 2016;12(7):e1006135.

[45] Waldmann TA. Protein-losing enteropathy. Gastroenterology 1966;50(3):422–43.

[46] Suzuki T. Regulation of intestinal epithelial permeability by tight junctions. Cell Mol Life Sci 2013;70(4):631–59.

[47] Campanacci V, Nurizzo D, Spinelli S, Valencia C, Tegoni M, Cambillau C. The crystal structure of theEscherichia colilipocalin Blc suggests a possible role in phospholipid binding. FEBS Lett 2004;562(1-3):183–8.

[48] Lee JM, Park SJ, Im DS. Calcium signaling of lysophosphatidylethanolamine through LPA1 in human SH-SY5Y neuroblastoma Cells. Biomol Therap 2017;25(2):194–201.

[49] Lee SJ, Leoni G, Neumann PA, Chun J, Nusrat A, Yun CC. Distinct phospholipase C-beta isozymes mediate lysophosphatidic acid receptor 1 effects on intestinal epithelial homeostasis and wound closure. Mol Cell Biol 2013;33(10):2016–28.

[50] Lin S, Han Y, Jenkin K, Lee S, Sasaki M, Klapproth JA, et al. Lysophosphatidic acid receptor 1 is important for intestinal epithelial barrier function and susceptibility to colitis. Am J Pathol 2017;188(2):353–66.

[51] Wijeratne SSK, Cuppett SL. Hydrogen peroxide induced oxidative stress damage and antioxidant enzyme response in Caco-2 human colon cells. J Agric Food Chem 2005;53(12):4476–81.

[52] Matter K, Balda MS. Signalling to and from tight junctions. Nat Rev Mol Cell Biol 2003;4(3):225–36.

[53] Lloydprice J, Investigators I, Arze C, Ananthakrishnan AN, Schirmer M, Avilapacheco J, et al. Multi-omics of the gut microbial ecosystem in inflammatory bowel diseases. Nature 2019;569(7758):655–62.

[54] Nakagawa S, Matsumoto M, Katayama Y, Oguma R, Wakabayashi S, Nygaard T, et al. Staphylococcus aureus virulent PSMalpha peptides induce keratinocyte alarmin release to orchestrate IL-17-dependent skin inflammation. Cell Host Microbe 2017;22(5):667–77 e5.

[55] Tsai PY, Zhang B, He WQ, Zha JM, Odenwald MA, Singh G, et al. IL-22 upregulates epithelial claudin-2 to drive diarrhea and enteric pathogen clearance. Cell Host Microbe 2017;21(6):671–81 e4.

[56] Seo SU, Kamada N, Munoz-Planillo R, Kim YG, Kim D, Koizumi Y, et al. Distinct commensals induce interleukin-1beta via NLRP3 inflammasome in inflammatory monocytes to promote intestinal inflammation in response to injury. Immunity 2015;42(4):744–55.

[57] Lin ME, Herr DR, Chun J. Lysophosphatidic acid (LPA) receptors: signaling properties and disease relevance. Prostaglandins Other Lipid Mediat 2010;91 (3-4):130–8.

[58] Li C, Dandridge KS, Di A, Marrs KL, Harris EL, Roy K, et al. Lysophosphatidic acid inhibits cholera toxin-induced secretory diarrhea through CFTR-dependent protein interactions. J Exp Med 2005;202(7):975–86.

[59] Singla A, Dwivedi A, Saksena S, Gill RK, Alrefai WA, Ramaswamy K, et al. Mechanisms of lysophosphatidic acid (LPA) mediated stimulation of intestinal apical Cl-/OH- exchange. Am J Physiol Gastrointest Liver Physiol 2010;298(2): G182–9.

[60] Emo J, Meednu N, Chapman TJ, Rezaee F, Balys M, Randall T, et al. Lpa2 is a negative regulator of both dendritic cell activation and murine models of allergic lung inflammation. J Immunol 2012;188(8):3784–90.

[61] Rhim JH, Jang IS, Yeo EJ, Song KY, Park SC. Role of protein kinase C-dependent A-kinase anchoring proteins in lysophosphatidic acid-induced cAMP signaling in human diploid fibroblasts. Aging Cell 2006;5(6):451–61.

[62] Balda MS, Gonzalezmariscal L, Matter K, Cereijido M, Anderson JM. Assembly of the tight junction: the role of diacylglycerol. J Cell Biol 1993;123(2):293–302.

[63] Basuroy S, Seth A, Elias BC, Naren AP, Rao R. MAPK interacts with occludin and mediates EGF-induced prevention of tight junction disruption by hydrogen peroxide. Biochem J 2006;393(1):69–77.

[64] Sheth P, Samak G, Shull JA, Seth A, Rao R. Protein phosphatase 2A plays a role in hydrogen peroxide-induced disruption of tight junctions in Caco-2 cell monolayers. Biochem J 2009;421(1):59–70.